NASA TECHNICAL MEMORANDUM

NASA TM X-3563

NASA TM X-3563

HEAT-TRANSFER AND PRESSURE MEASUREMENTS ON A SIMULATED ELEVON DEFLECTED 30° NEAR FLIGHT CONDITIONS AT MACH 7

Charles B. Johnson, Allan H. Taylor, and Irving Weinstein

Langley Research Center
Hampton, Va. 23665

NATIONAL AERONAUTICS AND SPACE ADMINISTRATION · WASHINGTON, D. C. · SEPTEMBER 1977

1. Report No.	2. Government Accession No.	3. Recipient's Catalog No.
NASA TM X-3563		

4. Title and Subtitle	5. Report Date
HEAT-TRANSFER AND PRESSURE MEASUREMENTS ON A SIMULATED ELEVON DEFLECTED 30° NEAR FLIGHT CONDITIONS AT MACH 7	September 1977
	6. Performing Organization Code

7. Author(s)	8. Performing Organization Report No.
Charles B. Johnson, Allan H. Taylor, and Irving Weinstein	L-11524
	10. Work Unit No. 505-11-31-02
9. Performing Organization Name and Address NASA Langley Research Center Hampton, VA 23665	11. Contract or Grant No.
	13. Type of Report and Period Covered Technical Memorandum
12. Sponsoring Agency Name and Address National Aeronautics and Space Administration. Washington, DC 20546	14. Sponsoring Agency Code

15. Supplementary Notes
Charles B. Johnson and Irving Weinstein: Langley Research Center.
Allan H. Taylor: Vought Corporation, Hampton, Virginia.

16. Abstract

Heat-transfer rates and pressures were obtained on an elevon plate (deflected 30°) and a flat plate upstream of the elevon in the Langley 8-foot high-temperature structures tunnel. The tests duplicated the flight Reynolds number and flight total enthalpy for altitudes of 26.8 km (88 000 ft) and 28.7 km (94 000 ft) at Mach 7. The heat-transfer and pressure data were used to establish heating and pressure loads that would be experienced during tests in the same facility of thermal protection system panels geometrically similar to the plate configuration of this study. The measured heating was compared with several theoretical predictions, and the closest agreement was obtained with a Schultz-Grunow reference enthalpy method of calculation.

17. Key Words (Suggested by Author(s))	18. Distribution Statement
Heat transfer Elevon Hypersonic flight Pressure levels	Unclassified - Unlimited Subject Category 34

19. Security Classif. (of this report)	20. Security Classif. (of this page)	21. No. of Pages	22. Price*
Unclassified	Unclassified	34	$4.00

* For sale by the National Technical Information Service, Springfield, Virginia 22161

HEAT-TRANSER AND PRESSURE MEASUREMENTS ON A SIMULATED ELEVON DEFLECTED 30° NEAR FLIGHT CONDITIONS AT MACH 7

Charles B. Johnson, Allan H. Taylor,*
and Irving Weinstein
Langley Research Center

SUMMARY

Heat-transfer rates and pressures were obtained on an elevon plate (deflected 30°) and a flat plate upstream of the elevon in the Langley 8-foot high-temperature structures tunnel. The tests duplicated the flight Reynolds number and flight total enthalpy for altitudes of 26.8 km (88 000 ft) and 28.7 km (94 000 ft) at Mach 7. The heat-transfer and pressure data were used to establish heating and pressure loads that would be experienced during tests in the same facility of thermal protection system panels geometrically similar to the plate configuration of this study. The measured heating was compared with several theoretical predictions, and the closest agreement was obtained with a Schultz-Grunow reference enthalpy method of calculation.

INTRODUCTION

A major problem associated with hypersonic flight is the high heating rates encountered in interaction areas where there is a large deflection of the flow, such as on speed brakes or control surfaces. Shown in figure 1 is a photograph of a model of a hypersonic research aircraft with the elevon locations indicated on the trailing edges of the swept wings. When the elevon is deflected, the large pressure increase which occurs on the windward surface, coupled with flow interaction, causes a significant increase in heating on the elevon surface. This increased heating must be considered in the design of the thermal protection system (TPS) for the control surface of a hypersonic research aircraft.

To evaluate various TPS systems proposed for the elevon of a hypersonic research aircraft, the actual heating experienced by the TPS material installed on a simulated wing-elevon must be determined for a fully developed turbulent boundary layer. For this purpose, two calibration plates were used to simulate (1) a wing (upstream plate) at 0° and -5° (compression) relative to the flow and (2) an elevon deflected 30° relative to the upstream plate. The two calibration plates were tested in the Langley 8-foot high-temperature structures tunnel near flight conditions. This report presents results of the heating and pressure tests.

The wind-tunnel tests closely duplicated the nominal flight conditions of Mach 7, at dynamic pressures of 47.9 kPa (1000 psf) and 59.9 kPa (1250 psf) at altitudes of 28.7 km (94 000 ft) and 26.8 km (88 000 ft), respectively, for val-

---

*Vought Corporation, Hampton, Virginia.

ues of total enthalpy near the flight values. The Reynolds number for the wind-tunnel tests was about 8.0×10^6 based on the distance from the leading edge to the elevon hinge line. For the full-scale aircraft shown in figure 1 (see ref. 1), the flight Reynolds number based on the distance from the leading edge to the hinge line at the outboard portion of the 70° swept wing would be about 13.0×10^6. Thus, the tunnel tests closely simulate the flight environment. Tests (three test runs) were conducted at two nominal tunnel conditions and two configuration settings.

SYMBOLS

Measurements and calculations were made in U.S. Customary Units and are presented in both the International System of Units (SI) and U.S. Customary Units.

C_f	local skin-friction coefficient
H	total enthalpy
H_{pk}	ratio of peak disturbed heat-transfer coefficient to undisturbed heat-transfer coefficient
h	static enthalpy
L	normalizing factor for longitudinal distance, 25.4 cm (10 in.)
M	Mach number
N_r	recovery factor
$N_{St,e}$	Stanton number evaluated at edge of boundary layer
P_{pk}	ratio of peak disturbed pressure to undisturbed pressure
p	pressure, kPa (psf)
q	dynamic pressure, kPa (psf)
$\dot{q}$	heating rate, W/m^2 (Btu/ft^2-sec)
$\dot{q}_o$	normalizing factor for heating rate, 11.35 kW/m^2 (1.0 Btu/ft^2-sec)
R	unit Reynolds number, per meter (per foot)
R_{AF}	Reynolds analogy factor
$R_{e,x}$	Reynolds number evaluated at edge of boundary layer based on streamwise surface distance x
T	temperature, K ($^\circ R$)
t	time, equal to 0 at start of heating, sec

x streamwise surface distance from plate leading edge, cm (in.)

$\bar{x}$ radial direction from center of thermocouple (see fig. 9), mm (in.)

$\bar{y}$ in-depth direction measured from plate surface (see fig. 9), mm (in.)

α angle of attack of panel holder, deg

ϵ deflection of elevon relative to plate upstream of hinge line, deg

μ viscosity of flow

ρ density

Subscripts:

aw adiabatic wall

e edge of boundary layer

i incompressible value

t total

w wall

∞ free-stream conditions

Abbreviation:

8-ft HTST Langley 8-foot high-temperature structures tunnel

Primes denote evaluation at reference enthalpy given by equation (3).

APPARATUS AND TEST PROCEDURES

Wind Tunnel

The model was tested in the aerothermal environment of the Langley 8-foot high-temperature structures tunnel (8-ft HTST). This tunnel is a hypersonic blowdown type that closely simulates the flight enthalpy and Reynolds number at Mach 6 to 7 at altitudes from 24.4 km (80 000 ft) to 39.6 km (130 000 ft) for test times up to 2 min. The test medium is generated by combustion of methane and air in a high-pressure combustor, and the reaction products are then expanded through an axisymmetric contoured nozzle to a nominal exit Mach number of 7. The nozzle has an exit diameter of 2.44 m (8.0 ft); however, the uniform core is about 1.22 m (4.0 ft) in diameter. The flow exits the nozzle as an open jet for 4.27 m (14 ft) and then enters a supersonic diffuser. Downstream of the supersonic diffuser, there is a single-stage annular air ejector. The flow from the ejector mixes with the hot gases in a long straight mixing tube and is then decelerated by a conical frustrum-type diffuser.

Test models are mounted in a large panel holder apparatus attached to a sting and are retracted and covered during wind-tunnel startup and shutdown. Insertion and retraction of a model is accomplished by an injection system which fully inserts the sled in less than 2 sec. A side view of the test chamber is shown in figure 2. A more detailed description of the facility, the panel holder, and the measured aerothermal parameters may be found in references 2 and 3.

Panel Holder

The tests were conducted with the calibration plates installed in a 1.47-m by 3.00-m (58-in. by 118-in.) panel holder, which is a rectangular slab with a 20° bevel at the leading edge as shown schematically in figure 3. A large rectangular cutout through the panel holder shown in figure 4 can accommodate test panel sizes up to 107.6 cm by 152.1 cm (42.38 in. by 59.88 in.), with access to the back of the test panel through a removable plate on the lower surface of the panel holder. Boundary-layer trips made from 0.24-cm (0.094-in.) diameter stainless steel spheres, described in reference 3, were mounted on the panel holder. A photograph of the panel holder (fig. 5) shows the installed flat plate and elevon plate.

Models

Two stainless steel calibration plates, an elevon plate and a flat plate, were instrumented with thermocouples and pressure orifices to determine heating rates and pressures that would be experienced during tests in the 8-ft HTST by thermal protection systems (TPS) geometrically similar to the plate configuration. The two plates represent an elevon deflected 30° relative to the upstream plate (wing), with the entire system either at 0° or -5° (compression) relative to the free stream.

Elevon plate.- A sketch of the elevon plate, 50.8 cm by 50.8 cm by 1.27 cm (20.0 in. by 20.0 in. by 0.5 in.), is shown in figure 6. The plate, fabricated of AISI type 347 stainless steel, was instrumented with 39 pressure orifices (1.524 mm (0.060 in.) in diameter) and 13 chromel-alumel thermocouples (0.254-mm (0.010-in.) diameter wire); however, only 20 of the pressure orifices were monitored for these test runs. The elevon plate was attached with four clevis fittings to a steel frame that could be positioned by a pivoted support web. One clevis fitting was fixed and the others were able to move to allow for thermal expansion. Details of these components are shown in figure 7. A welded steel skirt covered the openings on the sides and trailing edge of the elevon plate. The skirt shielded the cavity under the elevon plate from the hot test medium. A separate seal assembly was used to close the gap between the elevon plate and the steel skirt.

Flat plate.- A sketch of the flat plate, showing the details of construction and instrumentation, is shown in figure 8. The plate, fabricated of AISI type 347 stainless steel, was located adjacent to and upstream of the elevon

plate, and was 52.20 cm by 84.71 cm by 1.27 cm (20.55 in. by 33.35 in. by 0.5 in.). It was instrumented with 21 chromel-alumel thermocouples (0.254-mm (0.010-in.) diameter wire) and 15 pressure taps (1.524 mm (0.060 in.) in diameter) and was mounted flush to the surface of the panel holder.

Test Conditions

This investigation consisted of three wind-tunnel tests. The conditions for these tests are given in table I. For all the tests, the elevon plate was positioned at a 30° angle of incidence relative to the surface of the flat plate. Test runs 1 and 2 were made with the panel holder at an angle of attack of 0° at nominal dynamic pressures of 47.9 kPa (1000 psf) and 59.9 kPa (1250 psf), respectively. For test run 3, conducted at a nominal dynamic pressure of 47.9 kPa (1000 psf), the panel holder was pitched down 5° (compression). The length of the tests was about 6 to 8 sec to limit the maximum elevon plate surface temperature to approximately 644 K (1160° R).

Thermocouple Installation

The two stainless steel calibration plates (see figs. 6 and 8) were instrumented with thermocouples for the purpose of obtaining heat-transfer data. Prior to installing the thermocouples, the highest heating to the elevon plate was estimated using (1) the flat-plate heating data of reference 3, (2) the oblique shock pressure rise, and (3) the heating amplification correlation,

$$H_{pk} = (P_{pk})^{0.85} \tag{1}$$

found in reference 4. The estimates of heating to the elevon plate indicated that heating rates of approximately 1.02 MW/m^2 (90.0 Btu/ft^2-sec) could be expected. At this level of heating, it was determined that the thin skin calorimeter technique (see ref. 5), with a skin thickness of 1.016 mm (0.040 in.), was unsuitable for measuring heat transfer because the thin skin would buckle. Thermocouples mounted on the back face of the relatively thick elevon plate would also produce unsuitable results, since for inverse heat conduction codes, the error amplifies with increasing in-depth distance between the thermocouple junction and the surface of the material. Therefore, the thermocouples were installed flush with the exposed surface of the elevon. In addition, since the level of heating just upstream of the elevon-plate hinge line was unknown, the thermocouples in the flat plate upstream of the elevon were installed in the same way.

The procedure for installing the thermocouples consisted of drilling a 0.635-mm (0.025-in.) radius hole through the plate and countersinking the hole to a 0.889-mm (0.035-in.) radius on the plate surface. The thermocouple wires (0.254 mm (0.010 in.) in diameter) were drawn through the hole, formed into a spherical shape at the hot junction, and then peened flush to the plate surface in the countersunk hole. A sketch of a thermocouple installation is shown in figure 6.

DATA REDUCTION AND ANALYSIS

Data Reduction

Pressures on the two plates (figs. 6 and 8) were measured with electrical-wire strain gages, and surface temperatures were measured with chromel-alumel thermocouples. Electrical outputs from the pressure gages and thermocouples were recorded on magnetic tape by an analog-to-digital data recording system at 20 points per second. The heating rates at the 34 thermocouple stations were calculated using an inverse solution for two-dimensional transient heat conduction. This inverse code reported in appendix A of reference 6 was originally set up to calculate the heating rate to a porous leading edge with blowing and required only a modified input to calculate the two-dimensional heating to a 1.27-cm (0.5-in.) thick plate. The heating rate as a function of time was calculated using the time-temperature history of the surface temperature as an input to the inverse code from the start of heating ($t = 0$) for a period of 5 sec. The two-dimensional heat conduction solution, which assumed no heat flow in the spanwise direction, was validated by applying the one-dimensional code of reference 7 and a thermal model which had no longitudinal heat conduction. Results from this well-known one-dimensional (in-depth heat conduction) code agreed well with those from the two-dimensional code.

Thermocouple Analysis

Prior to installation of the thermocouples, the transient heat conduction was calculated in the area of the thermocouple locations to determine the error in the thermocouple reading due to the hole located directly under the thermocouple hot junction. The mathematical model used in the transient heat conduction analysis (MITAS) from reference 8 is shown in figure 9. The cross-hatched portion of the mathematical model represents the thermocouple. For simplicity, a 0.508-mm by 0.762-mm (0.020-in. by 0.035-in.) rectangle is used in the mathematical model to represent one-half of a sectioned view of the thermocouple. The MITAS computer code calculated a nodal temperature for each block in figure 9.

The calculated results using the MITAS computer code of reference 8 and the mathematical model are shown in figure 10. The figure shows the calculated thermocouple reading as a function of time from the start of heating for a given initial cold wall heating rate. These initial cold wall heating rates are for an initial wall temperature of 294.4 K (530° R). For a given cold wall heating rate, the actual heating rate decreases as the wall temperature increases. However, it was assumed in the calculation that the heat-transfer coefficient does not vary with a change in wall temperature.

The calculated difference between the actual surface temperature and the temperature that the thermocouple would indicate is shown in figure 11. This temperature difference was obtained at $t = 4.0$ sec from the difference between the calculated thermocouple temperature (fig. 10) and the surface nodal temperature of the block farthest from the four thermocouple blocks in figure 9. A cold wall heating rate of 1.02 MW/m^2 (90.0 Btu/ft^2-sec) indicates a temperature difference after 4.0 sec of heating of approximately 28 K (50.4° R). The error incurred by this temperature difference is shown in figure 12 as the percent

error in the absolute temperature. A cold wall heating rate of 1.02 MW/m^2 (90.0 Btu/ft^2-sec) results in a 5.2-percent error. This error in the thermocouple reading, when unaccounted for in the transient heat conduction code used in data reduction gives a heating rate that is slightly higher than the actual value.

Estimates of Heating to an Elevon

Calculations of surface temperature as a function of time were made using the transient heat conduction code (CAVE) of reference 9. These calculations were made in a one-dimensional mode for various initial cold wall heating rates as shown in figure 13. These are the heating rates that would be experienced by an elevon, at a free-stream Mach number of about 7, deflected from 0° to 40° over a range of dynamic pressure from 47.9 kPa (1000 psf) to 71.8 kPa (1500 psf). The heating rates that correspond to the test conditions are indicated for the flat plate ($\alpha = -5°$ not shown) and for the elevon plate. The additional curves in figure 13 give a more detailed variation of surface temperature as a function of initial cold wall heating rate. An estimate of the length of the run had to be made to limit the surface temperature to approximately 644 K (1160° R). This estimate of run time was made from figure 13 for a given elevon deflection and a given dynamic pressure.

Figure 14 shows the cold wall and hot wall heating rates evaluated at $t = 4.0$ sec. The dashed cold wall curve was obtained from a cross plot of the cold wall heating rates and surface temperatures at $t = 4.0$ sec from figure 13. The hot wall curve was generated from the cold wall curve using the heat-transfer coefficient for a given cold wall heating rate, the surface temperature, and the adiabatic wall temperature associated with each cold wall heating rate. The adiabatic wall temperature varied from 1744 K (3140° R) to 1875 K (3375° R) for elevon deflections from 10° to 40°. The hot wall curve in figure 14 was used to make estimates of heating rates expected during the wind-tunnel tests and to calculate heating rate at 4.0 sec after the start of heating using the surface thermocouple temperature data at $t = 4.0$ sec.

RESULTS AND DISCUSSION

Pressure Distributions

The tunnel test conditions for the three test runs are shown in table I. The pressure distributions on the flat plate and elevon plate for test runs 1 and 2, at nominal dynamic pressures of 47.9 kPa (1000 psf) and 59.9 kPa (1250 psf) are shown in figures 15 and 16, respectively. For these two runs, the flat plate was set at 0° relative to the free stream and the elevon was deflected 30° relative to the flat plate. The pressures on the flat plate for these two test conditions were about 12 percent above the pressure expected on the plate due to displacement thickness effects of a turbulent boundary layer (the expected pressure due to displacement thickness effects (ref. 10) is $p_e/p_\infty \approx 1.11$). The pressures on the elevon rapidly increase in the area of the hinge line with approximately an 18-percent overshoot above the oblique shock value. Downstream of the peak value, the pressures decrease to approximately 12 percent below the oblique shock

level at the trailing edge of the elevon. The pressure distribution shown in figure 17 was obtained at a nominal dynamic pressure of 47.9 kPa (1000 psf), with the flat plate deflected down 5° (compression) relative to the free stream and an elevon deflection angle of 30° relative to the flat plate. In figure 17, the pressure level on the forward portion of the flat plate agrees with oblique shock theory, but the pressure on the flat plate increases rapidly near the hinge line and peaks at 26 percent above the oblique shock level on the elevon. The pressure then decreases to about 15 percent below oblique shock level at the trailing edge of the elevon.

Calculated Heating Rates at Flight Conditions

Heating rates expected in flight ($M_\infty = 6.9$ and $q_\infty = 47.9$ kPa (1000 psf)) on an elevon deflected 30° relative to the free stream were calculated for comparison with heating rates measured on the elevon plate. These flight heating rates were calculated by (1) the Schultz-Grunow reference enthalpy method and (2) the power-law heating amplification correlation (eq. (1)).

The Schultz-Grunow method starts with the incompressible form of skin friction (see ref. 11), which for a turbulent boundary layer is

$$\left(\frac{C_f}{2}\right)_i = 0.185(\log_{10} R_{e,x})^{-2.584} \tag{2}$$

The incompressible form of skin friction was made applicable to compressible flows by evaluating the local flow properties at a reference condition, defined from Eckert's reference enthalpy, which is

$$h' = 0.5(h_w + h_e) + 0.22(h_{aw} - h_e) \tag{3}$$

where $h_{aw} = h_e + N_r(H_e - h_e)$ and $N_r = 0.89$. The compressible skin friction was found from

$$\frac{C_f}{2} = 0.185\left(\frac{\rho'}{\rho_e}\right)\left[\log_{10}\left(R_{e,x}\,\frac{\rho'}{\rho_e}\,\frac{\mu_e}{\mu'}\right)\right]^{-2.584} \tag{4}$$

The local Stanton number was calculated from a modified form of the Reynolds analogy in the form

$$N_{St,e} = \frac{C_f}{2} R_{AF} \tag{5}$$

where R_{AF} is the Reynolds analogy factor. The method used to calculate the value of R_{AF} was the same method used in reference 12 where a modified form of the Reynolds analogy and the Spalding-Chi skin-friction theory were used to calculate heating. Local real-gas airflow properties on the elevon were calculated for conditions behind an oblique shock generated by the compression of the flow over a 30° wedge; the same real-gas program used in reference 12 was employed.

The power-law heating amplification correlation (eq. (1)) used the pressure amplification (P_{pk}) found for a 30° wedge compression and the undisturbed heating to the flat plate at 1.857 m (73.10 in.) from the leading edge (i.e., the distance to the hinge line of the model shown in fig. 4). The undisturbed heating to the flat plate was calculated for $M_\infty = 6.9$ and $q_\infty = 47.9$ kPa (1000 psf) using the Schultz-Grunow reference enthalpy method just described. The results of the calculations from the two methods are shown in figure 18.

Heat-Transfer Distributions

The results of the heating measurements on the flat plate and elevon plate for the three wind-tunnel tests (see table I) are shown in figures 19, 20, and 21. The circles represent the measured data reduced by the two-dimensional inverse heat conduction code (ref. 6). The solid line represents the fairing of data points obtained from measured surface temperatures and the calculations of a one-dimensional direct heat conduction code (ref. 9). In this method of data reduction, the measured surface temperatures were used along with the hot wall heating curve of figure 14 to obtain the one-dimensional conduction heating rates (i.e., at 4.0 sec after the start of heating). The dot-dashed curves in the three figures are fairings of the predictions of heating using the power-law heating amplification correlation (eq. (1)). To obtain the predictions of heating, the correlation used the average of five data points just upstream of the hinge line for the undisturbed value of heating and the actual pressure distributions on the elevon in figures 15, 16, and 17. The Schultz-Grunow reference enthalpy method of calculation is indicated by the dashed curves in the three figures and is the result of a real-gas airflow calculation using the measured pressures (figs. 15, 16, and 17) and the measured surface temperatures. This method of calculation is the same method used to make one of the flight calculations in figure 18. The local flow properties were calculated for the real-gas airflow field behind the oblique shock generated by the elevon plate.

In figure 19, the fairing of the data points obtained from the surface temperature and the one-dimensional conduction code of reference 9 (see fig. 14) agrees quite well with the data from the inverse code on both the flat plate and the elevon plate; however, the power-law correlation overpredicts the data by about 45 percent and the reference enthalpy method underpredicts the data by about 14 percent. The calculations shown in figure 18 were made for a nominal Mach number of 6.9 and a dynamic pressure of 47.9 kPa (1000 psf) which are similar to the flow conditions for the data in figure 19 (see table I). The data measured on the elevon plate in figure 19 and the flight predictions of heating in figure 18, using the reference enthalpy method, agree reasonably well over the downstream two-thirds of the elevon.

In figure 20, the fairing of the data obtained from the one-dimensional conduction theory of reference 9 (see fig. 14) and the surface temperature falls below the data from the inverse code on the flat plate by a large amount and on the elevon plate by a lesser amount. This discrepancy results from the assumption in the calculation method of reference 9 of a constant heat-transfer coefficient after a step input in heating. For this one test run, the heat-transfer coefficient was not constant for the first 4 sec of heating. This fact was recognized upon an inspection of the temperature-time plots from the thermocouples on

the surface of the flat plate. These plots indicate that for early times (t = 1 to 2 sec) the heat-transfer coefficient was much lower than at the time the data were evaluated (i.e., at t = 4 sec). The reason for the lower heat-transfer coefficient in the early part of the run is believed to be due to unsteady conditions in the facilities combustor. This condition was rectified at least 2 sec before the time the data were evaluated. The power-law correlation prediction of heating in figure 20 overpredicts the data by about 36 percent, while the reference enthalpy method underpredicts by about 20 percent.

In figure 21, the data obtained from the one-dimensional code of reference 9 (see fig. 14) agree reasonably well with the data from the inverse code on both the flat plate and the elevon plate. The power-law correlation overpredicts the data by approximately 47 percent, while the reference enthalpy method underpredicts the data by approximately 20 percent.

SUMMARY OF RESULTS

Measurements of heat transfer and pressure were made during three test runs in the Langley 8-foot high-temperature structures tunnel on two calibration plates. A flat plate was located upstream of an elevon plate deflected 30° relative to the flat plate. The measurements were made to predict the heating and pressure distributions during tests in the same facility of thermal protection system panels geometrically similar to the plate configuration of this report. The heat transfer was measured with thermocouples installed flush with the exposed surface of the elevon plate and upstream flat plate. The accuracy of thermocouples installed in this way was investigated using a direct two-dimensional heat conduction analysis. An error in the absolute temperature of 5.2 percent resulted for the estimated heating rates to the elevon plate. The temperature histories were reduced to heating rates using a two-dimensional inverse heat conduction code. One-dimensional conduction calculations were also made to determine the time of exposure to reach a given maximum surface temperature.

A simplified method of data reduction using a one-dimensional direct conduction code and the actual surface temperature at a given time from the start of heating, agreed well with the data from a complete inverse two-dimensional heat conduction code.

Comparisons between the experimental data from the three runs and various theoretical calculations indicated the following:

(1) The measured pressure distributions on the elevon plate are greater than the oblique shock value near the hinge line and decrease along the elevon length to a pressure less than the oblique shock value at the trailing edge of the elevon plate.

(2) The power-law heating amplification correlation overpredicted the heat-transfer rates by 36 to 47 percent.

(3) The heating rates predicted from the Schultz-Grunow reference enthalpy theory are lower than the experimental results by 14 to 20 percent.

(4) Real-gas heating calculations (Schultz-Grunow reference enthalpy method) for flight conditions on an elevon deflected 30° at Mach 6.9 and at a dynamic pressure of 47.9 kPa (1000 psf) agreed reasonably well with experimental data on the downstream two-thirds of the elevon plate taken at the same nominal Mach number and dynamic pressure.

Langley Research Center
National Aeronautics and Space Administration
Hampton, VA 23665
July 27, 1977

REFERENCES

1. Penland, Jim A.; Fournier, Roger H.; and Marcum, Don C.: Aerodynamic Characteristics of a Hypersonic Research Airplane Concept Having a 70° Swept Double-Delta Wing at Mach Numbers From 1.50 to 2.86. NASA TN D-8065, 1975.

2. Weinstein, Irving: Heat-Transfer and Pressure Distributions on Hemisphere-Cylinders in Methane-Air Combustion Products at Mach 7. NASA TN D-7104, 1973.

3. Deveikis, William D.; and Hunt, L. Roane: Loading and Heating of a Large Flat Plate at Mach 7 in the Langley 8-Foot High-Temperature Structures Tunnel. NASA TN D-7275, 1973.

4. Johnson, Charles B.; and Kaufman, Louis G., II: Interference Heating From Interactions of Shock Waves With Turbulent Boundary Layers at Mach 6. NASA TN D-7649, 1974.

5. Johnson, Charles B.: Heat-Transfer Measurements at Mach 8 on a Flat Plate With Deflected Trailing-Edge Flap With Effects of Transition Included. NASA TN D-5899, 1970.

6. Hunt, James L.; Bushnell, Dennis M.; and Beckwith, Ivan E.: The Compressible Turbulent Boundary Layer on a Blunt Swept Slab With and Without Leading-Edge Blowing. NASA TN D-6203, 1971.

7. Garrett, L. Bernard; and Pitts, Joan I.: A General Transient Heat-Transfer Computer Program for Thermally Thick Walls. NASA TM X-2058, 1970.

8. Connor, Robert J.; Adams, Jeanette A.; Shirley, Eugene; and Kannady, Roy E., Jr.: Martin Interactive Thermal Analysis System. MDS-SPLPD-71-FD238, Martin-Marietta Corp., Mar. 1971.

9. Rathjen, Kenneth A.: CAVE: A Computer Code for Two-Dimensional Transient Heating Analysis of Conceptual Thermal Protection Systems for Hypersonic Vehicles. NASA CR-2897, 1977.

10. Eckstrom, D. J.: Engineering Analysis of Boundary Layers and Skin Friction on Bodies of Revolution at Zero Angle of Attack. TM-21-21, Lockheed Missiles & Space Co., May 1965.

11. Schlichting, Hermann (J. Kestin, transl.): Boundary Layer Theory. Fourth ed. McGraw-Hill Book Co., Inc., c.1960.

12. Johnson, Charles B.; and Boney, Lillian R.: A Simple Integral Method for the Calculation of Real-Gas Turbulent Boundary Layers With Variable Edge Entropy. NASA TN D-6217, 1971.

TABLE I.- TEST CONDITIONS

(a) SI Units

Test run	α, deg	ε, deg	M_∞	q_∞, kPa	R_∞, per meter	Combustor pressure, MPa	Combustor temperature, K	p_∞, kPa	T_∞, K	T_{aw}/T_t
1	0	30	7.0	49.7	3.38×10^6	13.6	1912	1.43	228	0.956
2	0	30	6.7	61.0	4.30×10^6	16.7	1798	1.89	231	.955
3	-5	30	6.9	48.5	3.35×10^6	13.7	1924	1.43	230	.958

(b) U.S. Customary Units

Test run	α, deg	ε, deg	M_∞	q_∞, psf	R_∞, per foot	Combustor pressure, psia	Combustor temperature, $^\circ$R	p_∞, psia	T_∞, $^\circ$R	T_{aw}/T_t
1	0	30	7.0	1037	1.03×10^6	1977	3442	0.2072	410	0.956
2	0	30	6.7	1275	1.31×10^6	2429	3237	.2745	415	.955
3	-5	30	6.9	1013	1.20×10^6	1980	3464	.2078	414	.958

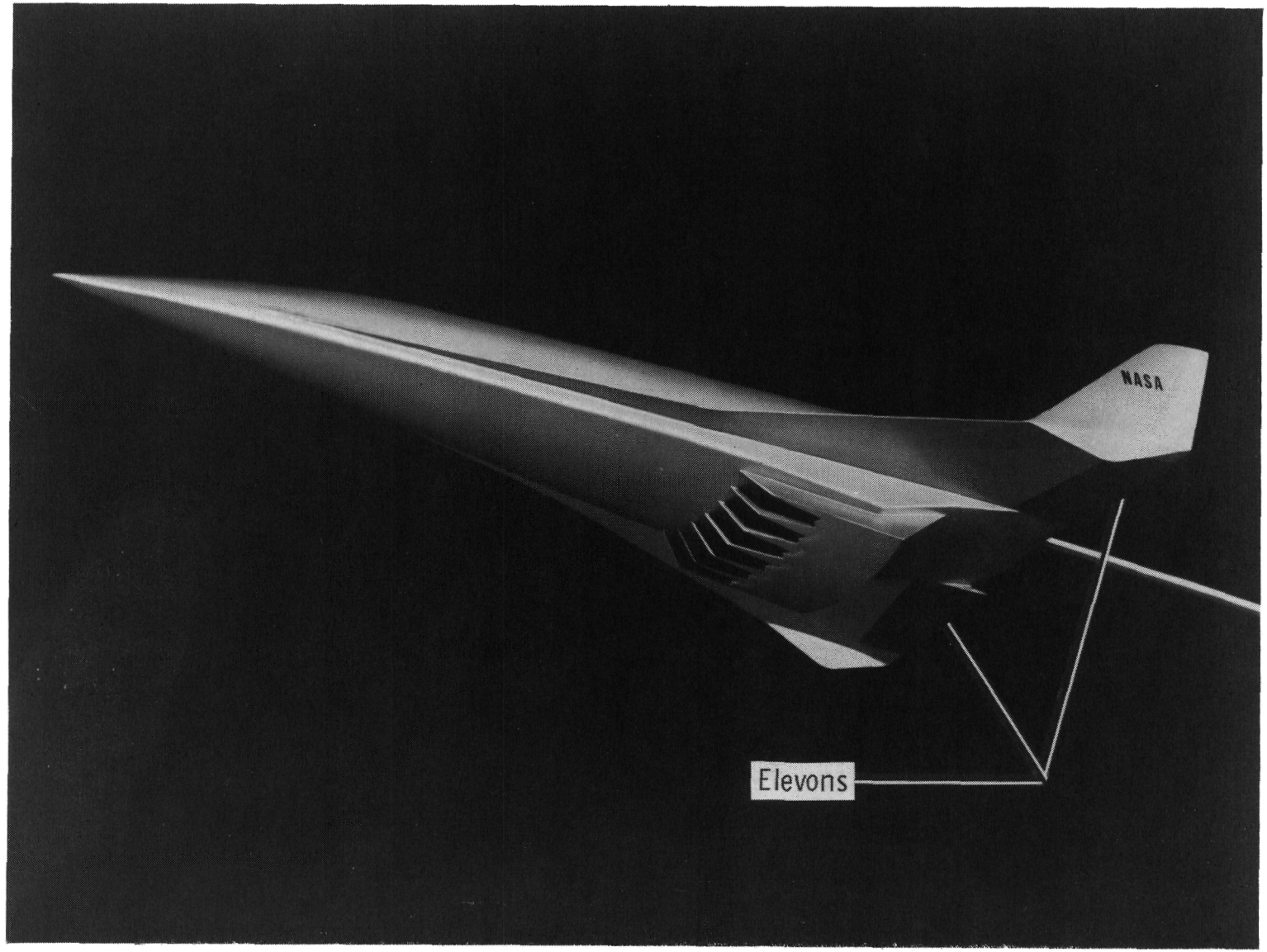

L-72-9147.1

Figure 1.- Model of hypersonic research aircraft.

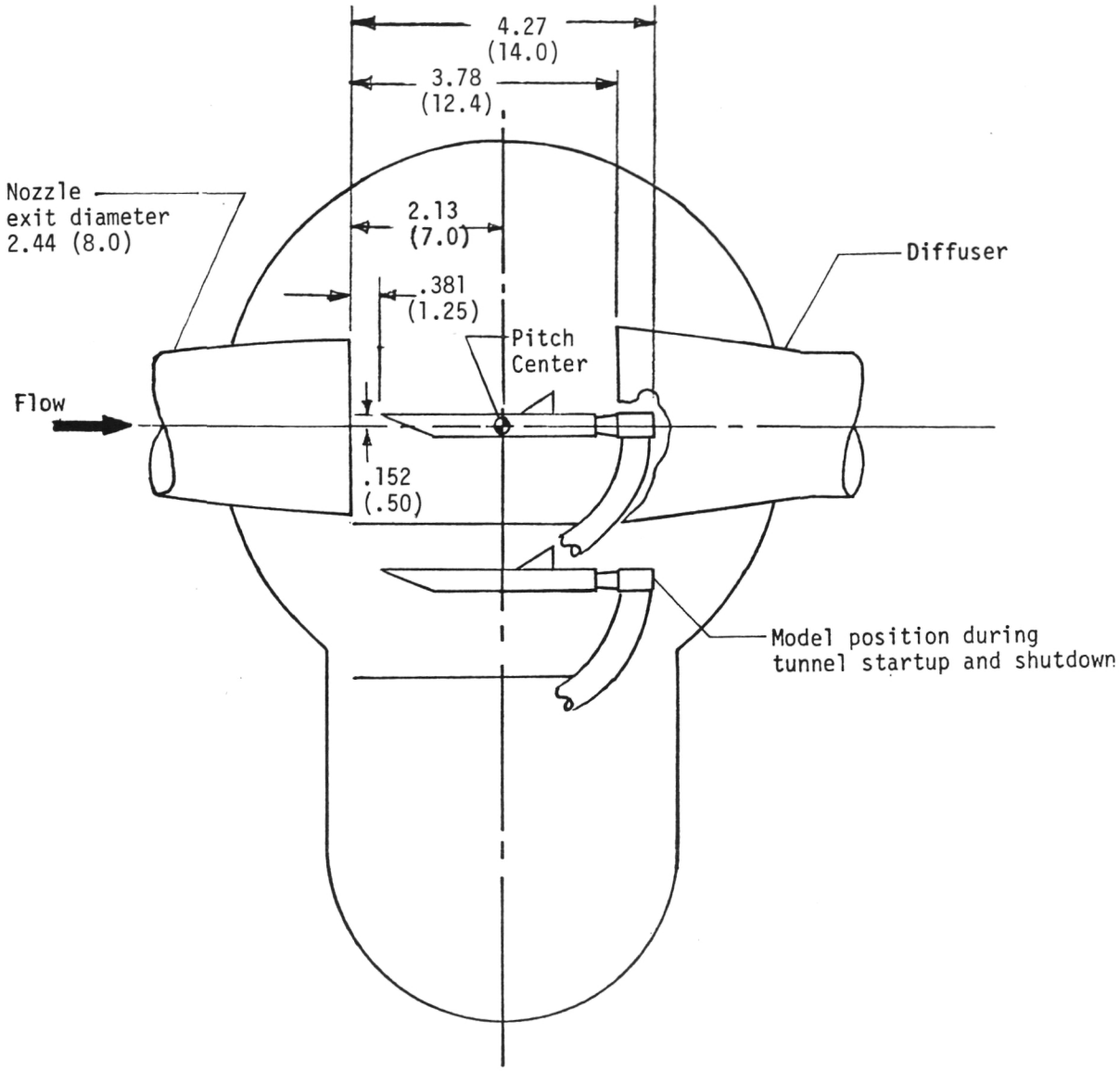

Figure 2.- Side view of test section of 8-ft HTST.
Dimensions are in meters (feet).

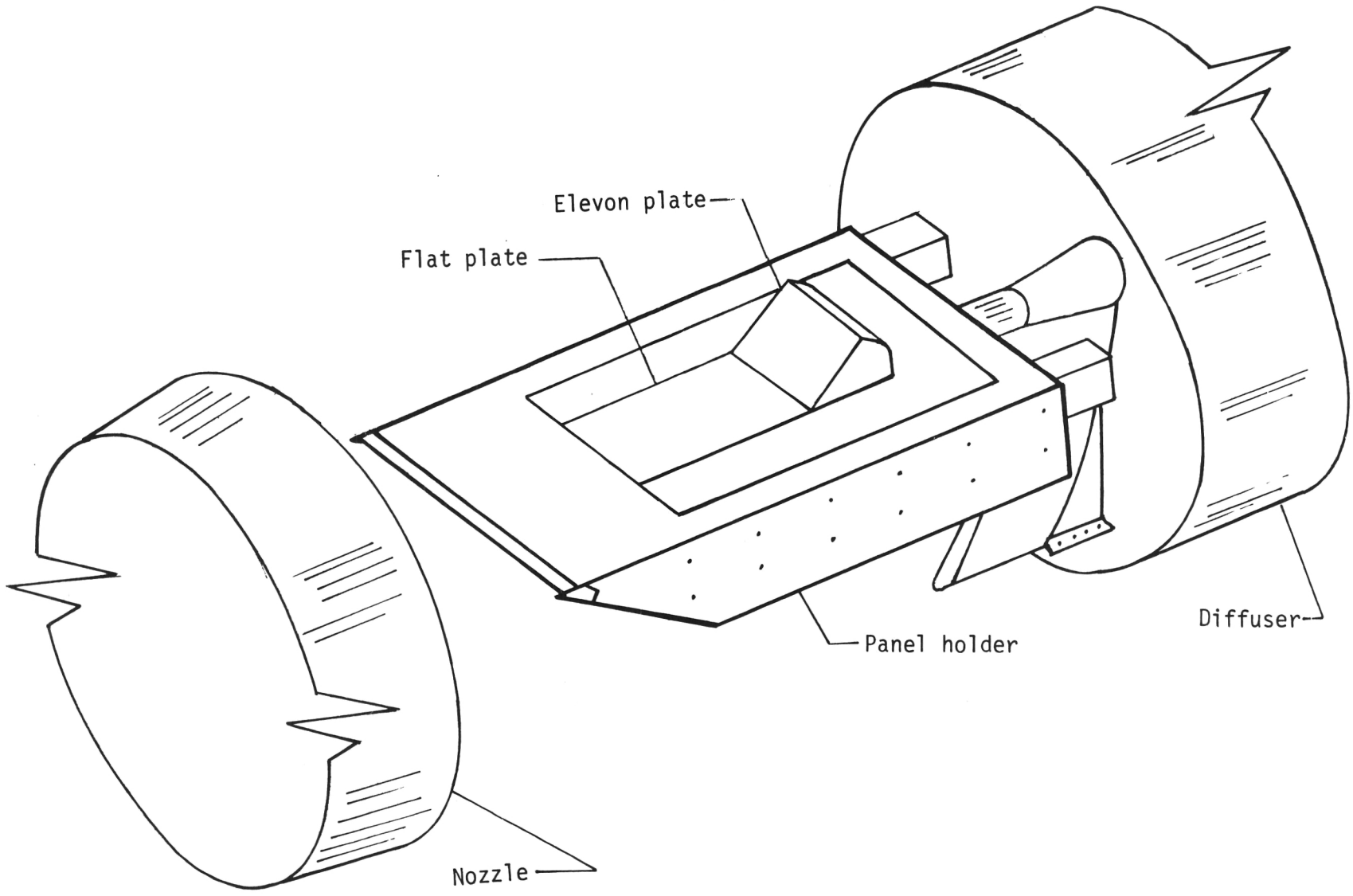

Figure 3.- Schematic of panel holder in test section of 8-ft HTST.

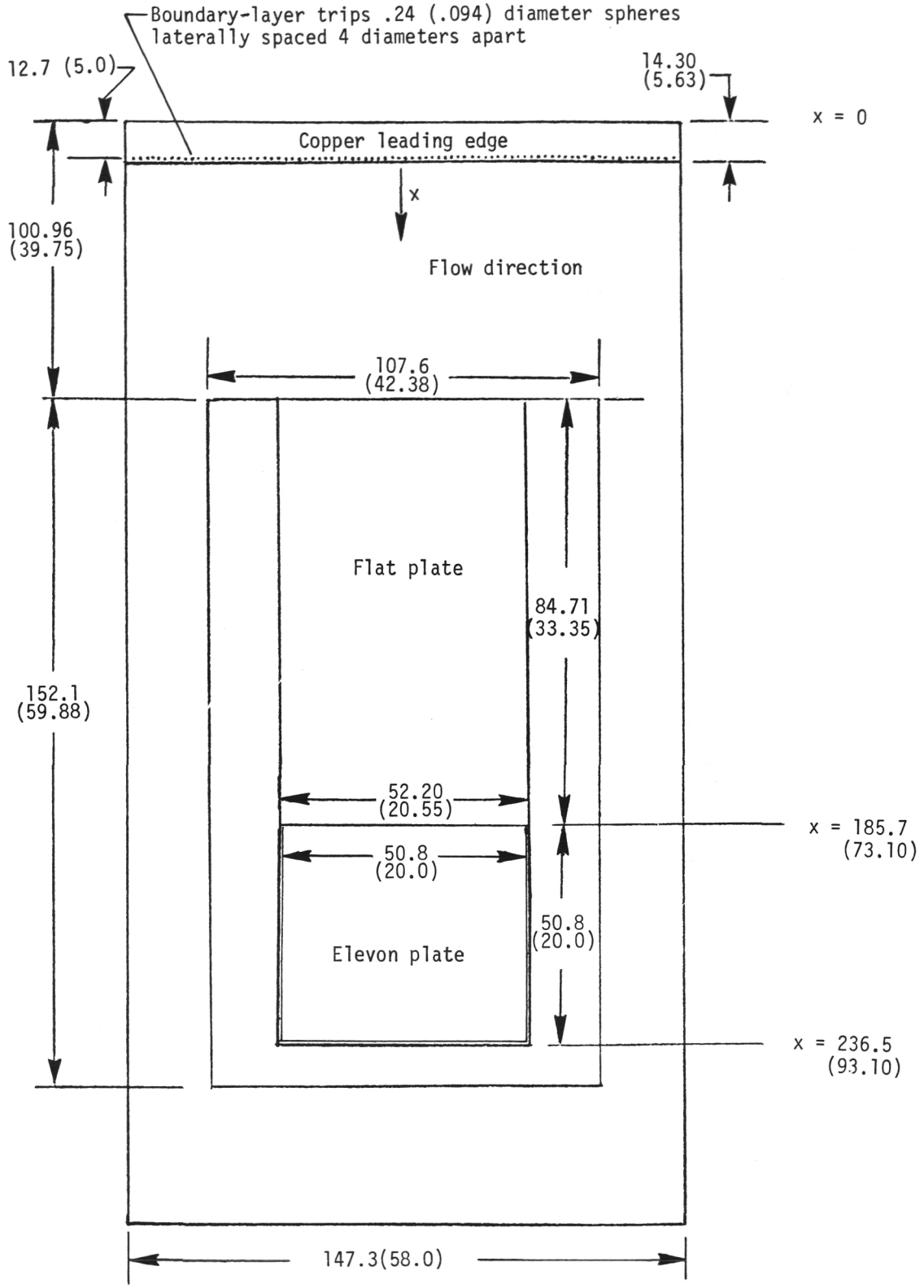

Figure 4.- Location of flat plate and elevon plate in panel holder. All dimensions are in centimeters (inches).

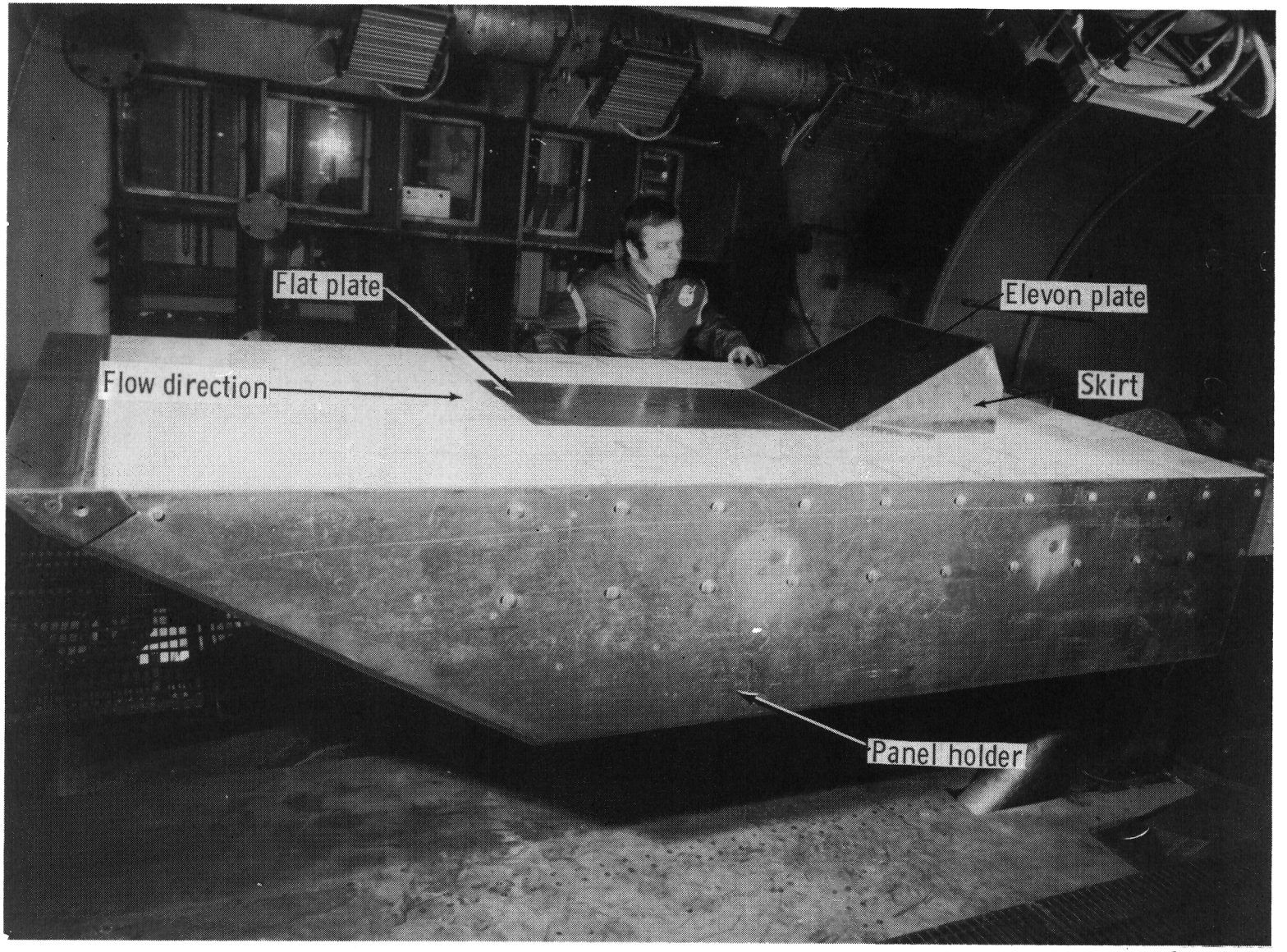

L-76-1088.1

Figure 5.- Panel holder installed in test section of 8-ft HTST.

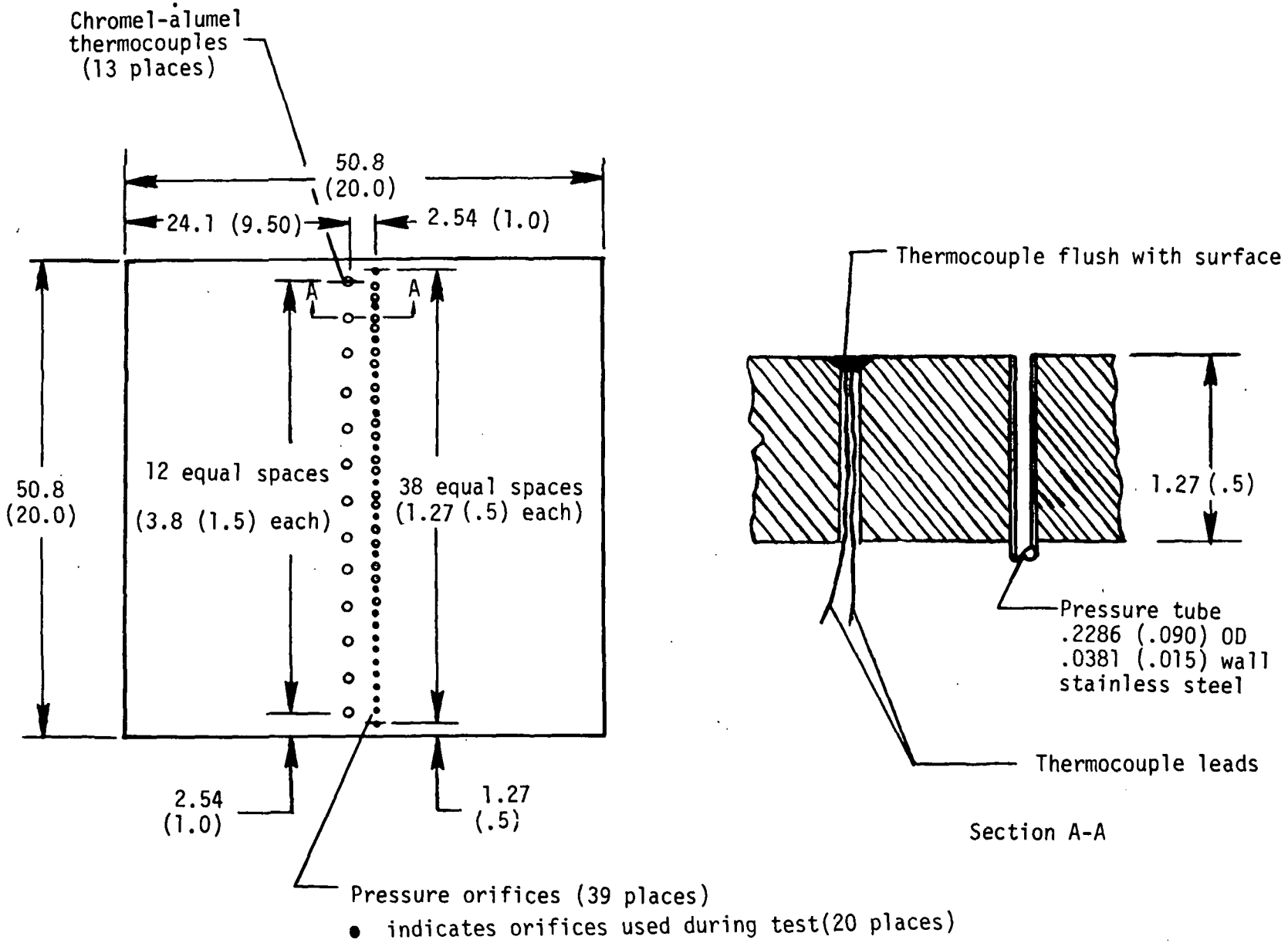

Figure 6.- Sketch of elevon plate. All dimensions are in centimeters (inches).

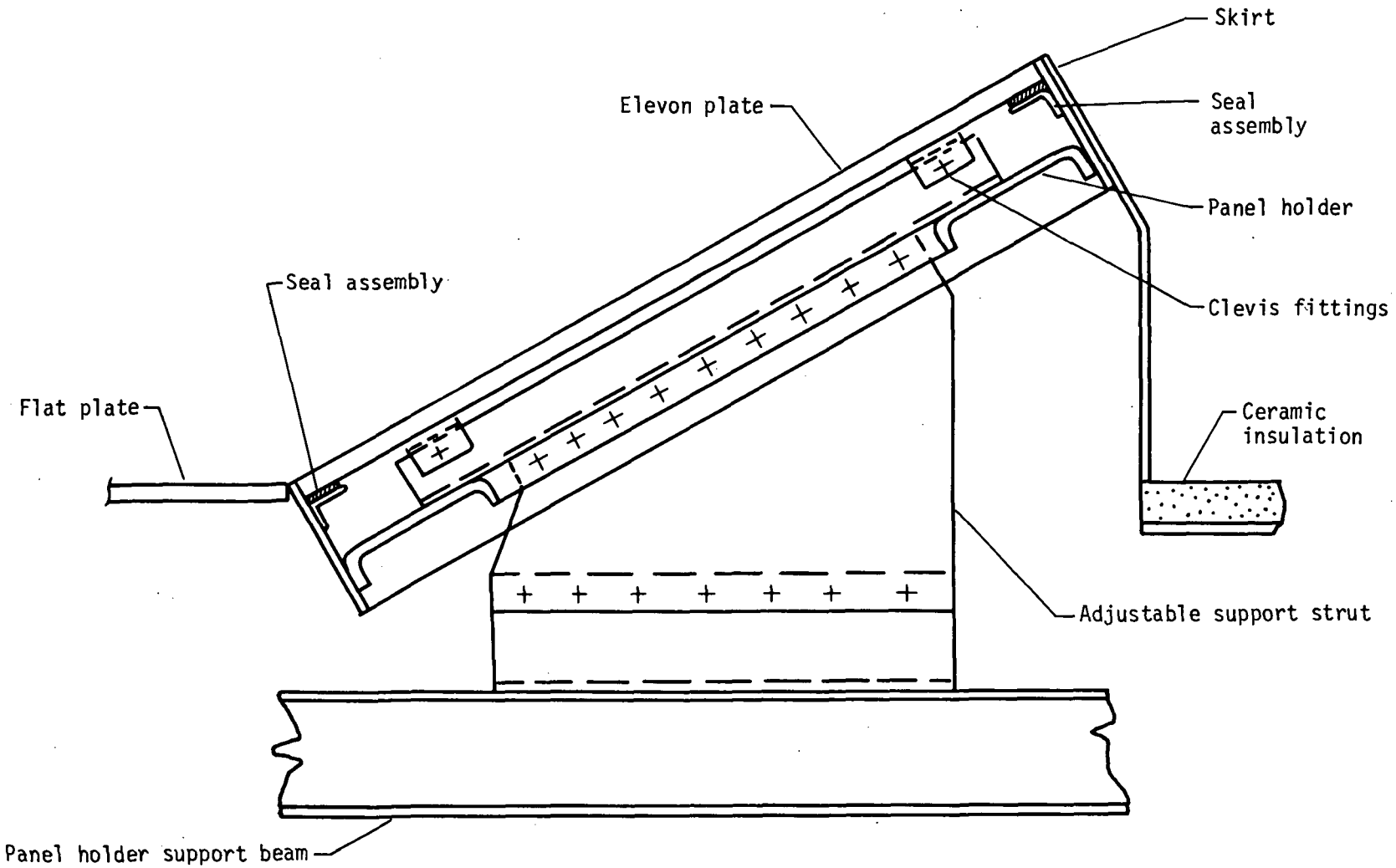

Figure 7.- Sketch of support apparatus for elevon plate.

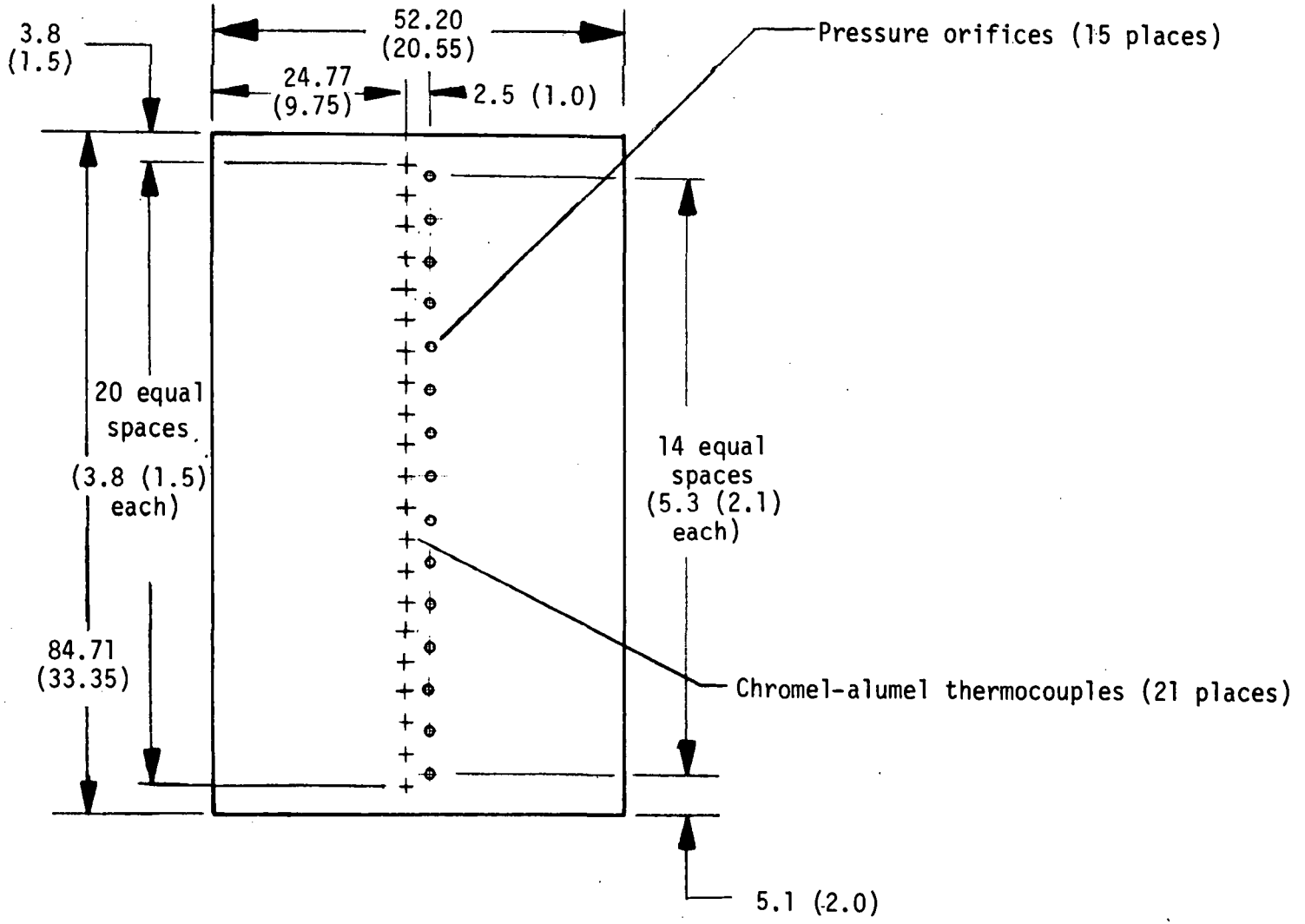

Figure 8.- Sketch of flat plate. All dimensions are in centimeters (inches).

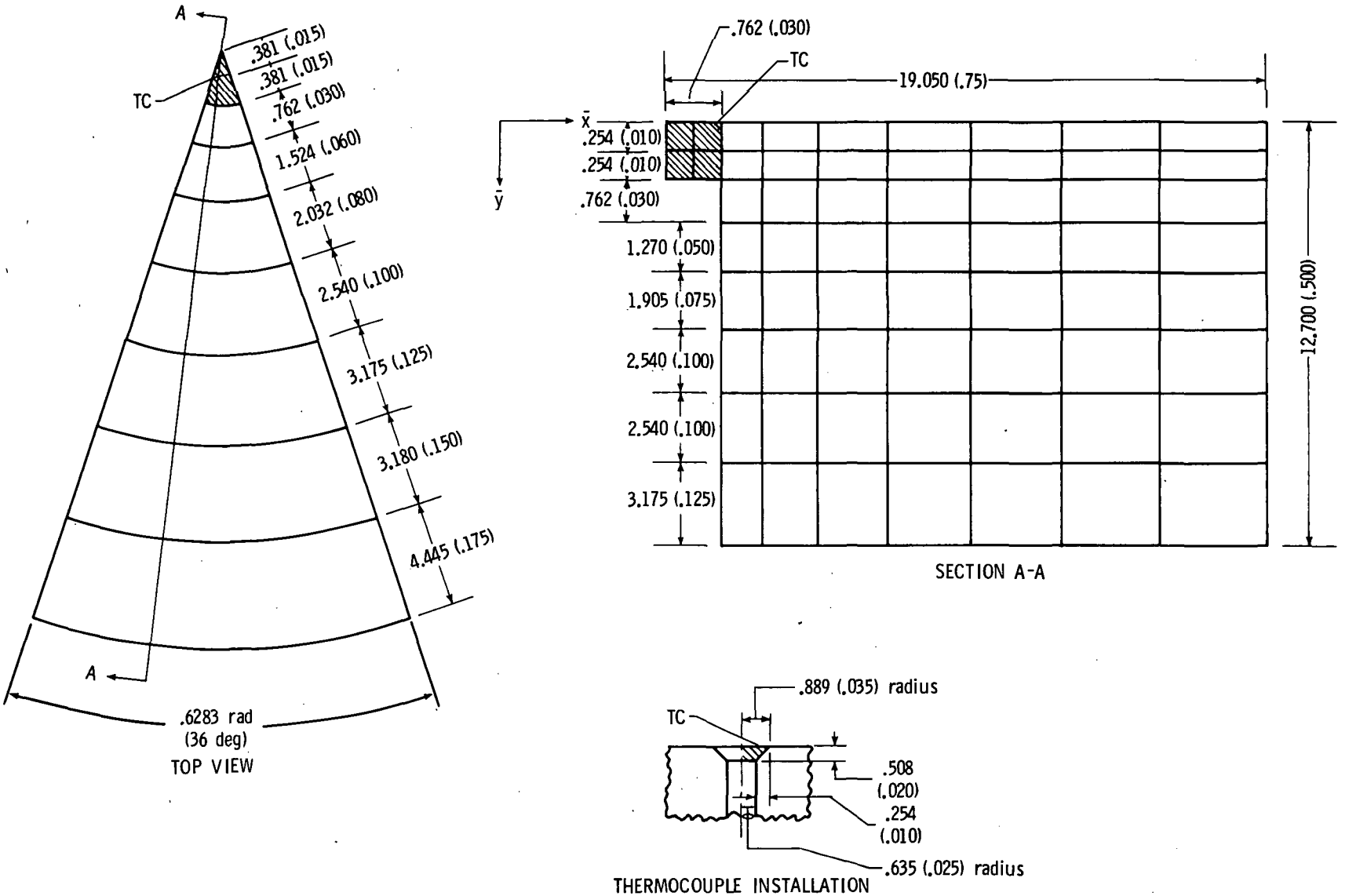

Figure 9.- Transient heat conduction mathematical model used for determining thermocouple (TC) error. All dimensions are in millimeters (inches) unless otherwise noted.

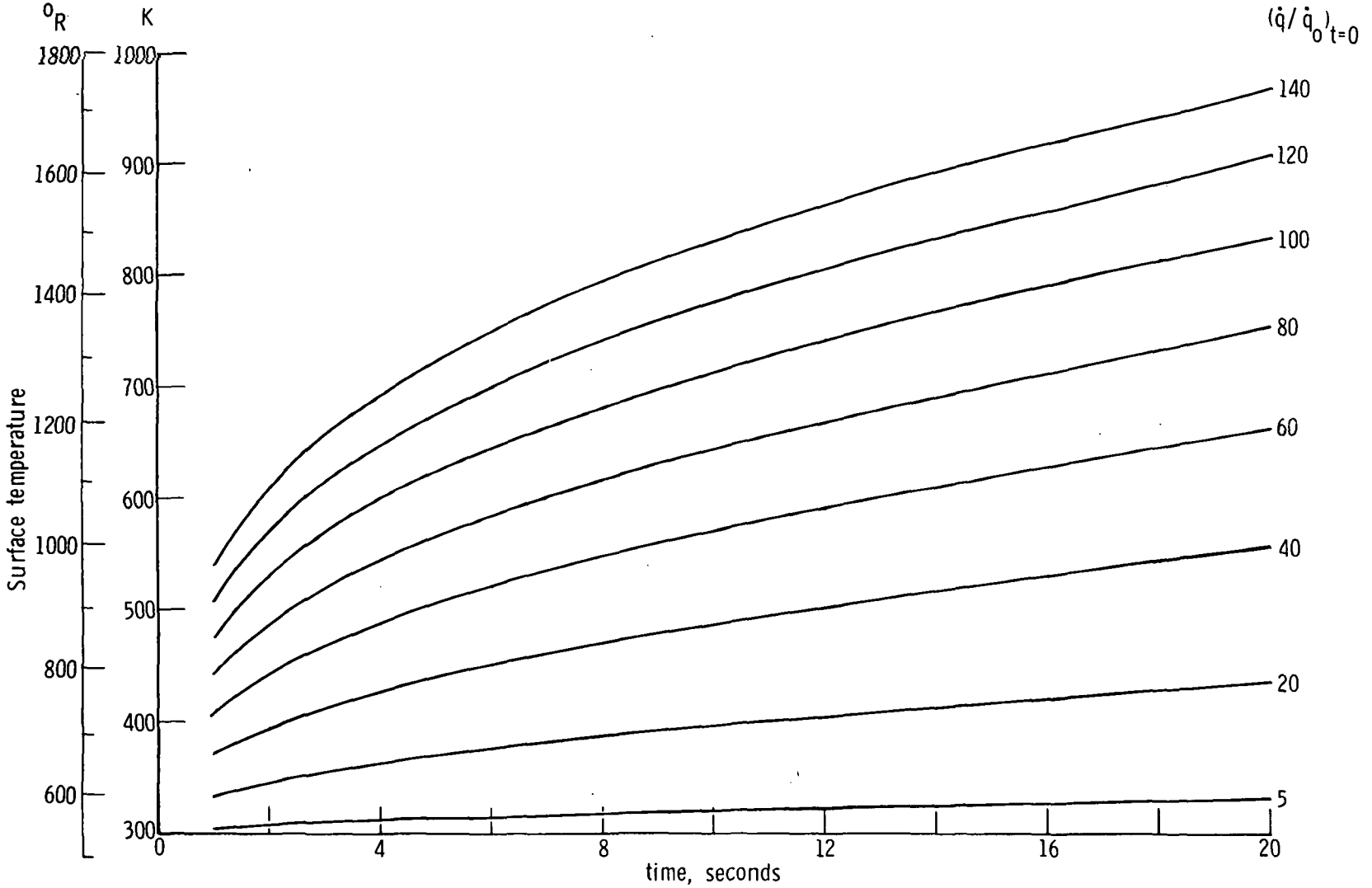

Figure 10.- Surface thermocouple temperature as a function of time for various cold wall heating rates calculated using code of reference 8. $\dot{q}_o$ = 11.35 kW/m^2 (1.0 Btu/ft^2-sec); 1.27-cm (0.5-in.) thick stainless steel plate; initial temperature, 294.4 K (530° R).

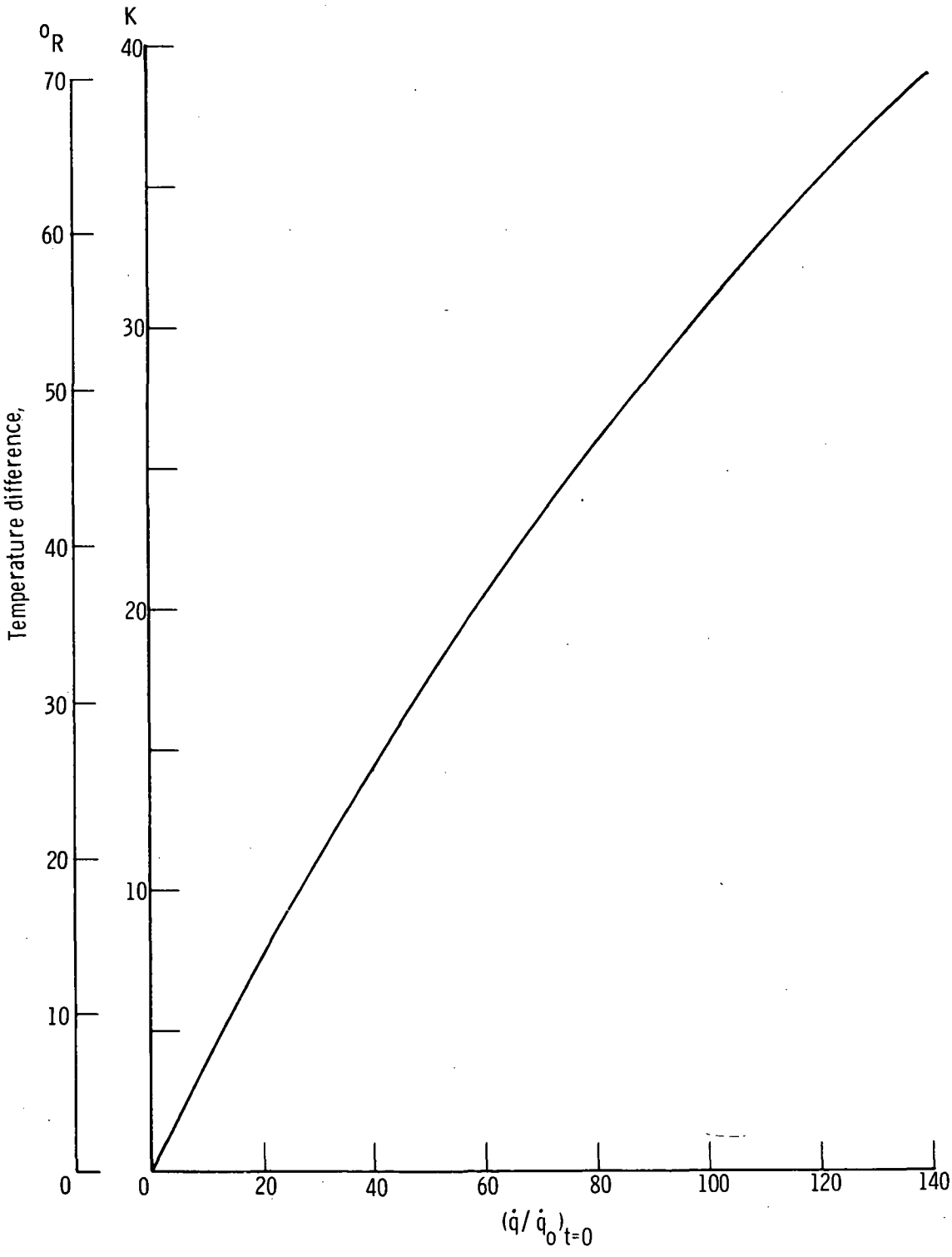

Figure 11.- Calculated difference between temperature of thermocouple and surrounding stainless steel surface as a function of heating rate. $\dot{q}_o$ = 11.35 kW/m^2 (1.0 Btu/ft^2-sec); t = 4.0 sec.

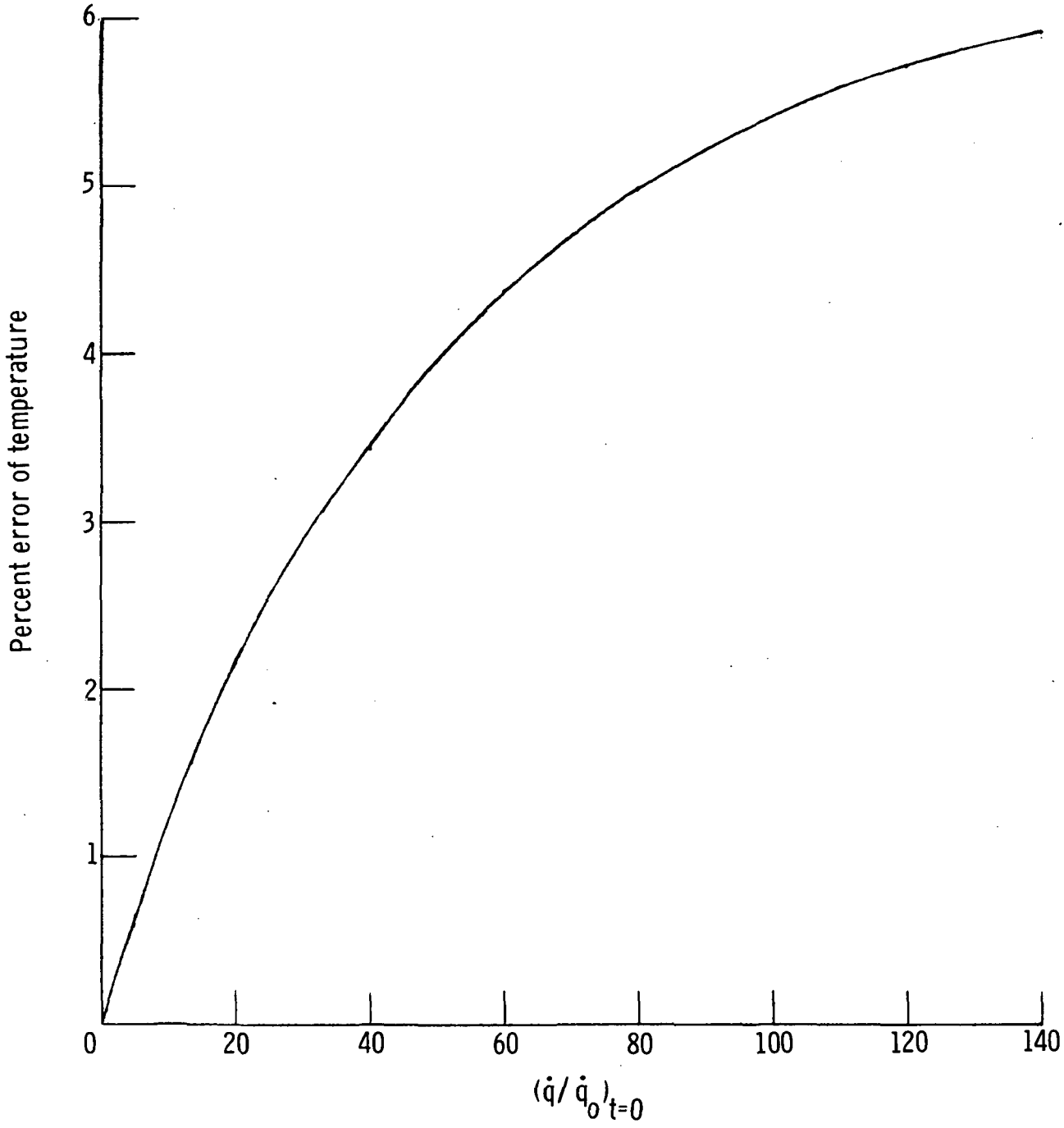

Figure 12.- Percent error of absolute temperature between thermocouple and surrounding stainless steel surface. $\dot{q}_o$ = 11.35 kW/m^2 (1.0 Btu/ft^2-sec); t = 4.0 sec.

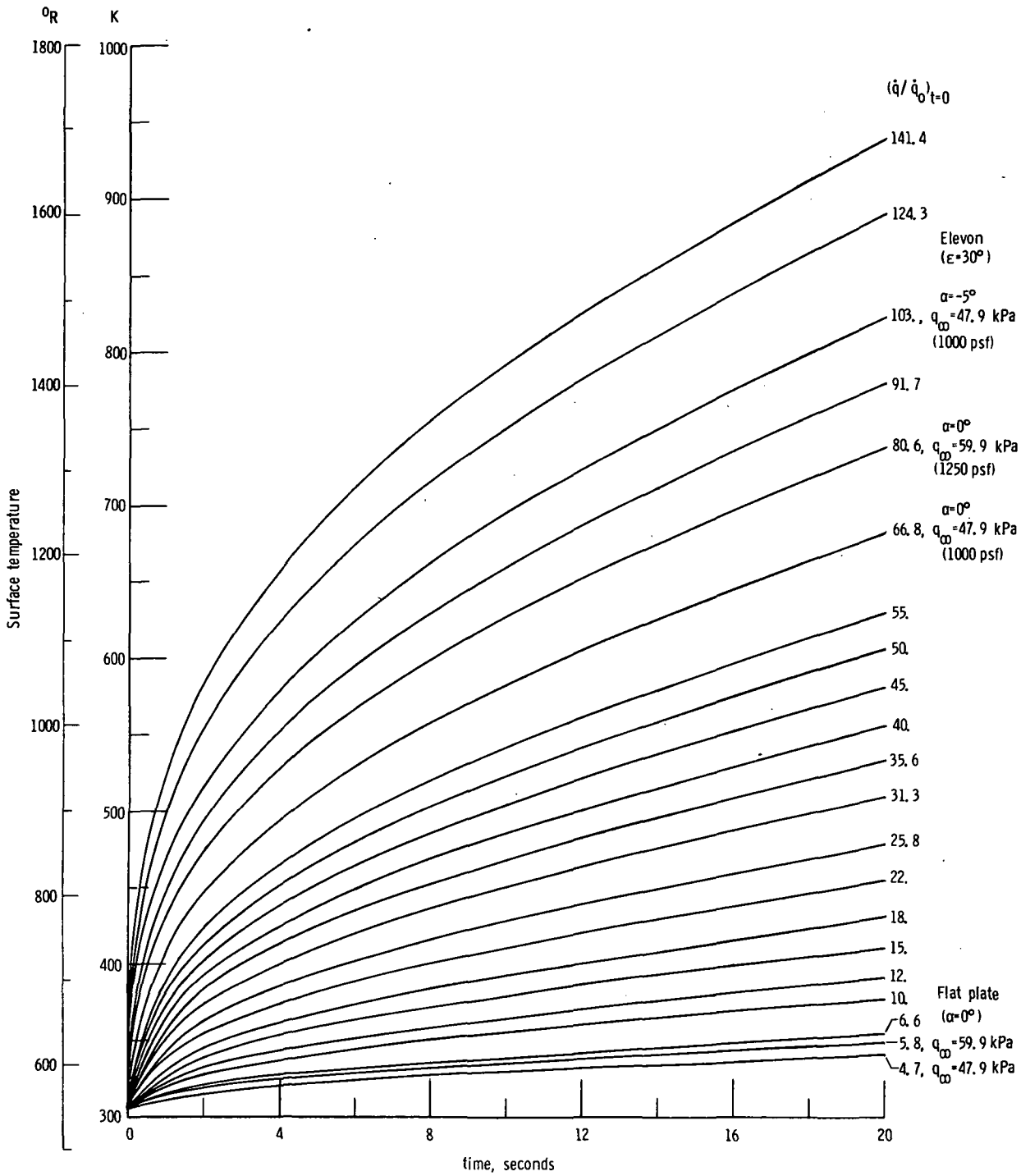

Figure 13.- Surface temperature as a function of time for various cold wall heating rates calculated using code of reference 9. $\dot{q}_o$ = 11.35 kW/m^2 (1.0 Btu/ft^2-sec). 1.27-cm (0.5-in.) thick stainless steel plate; initial temperature, 305.6 K (550° R).

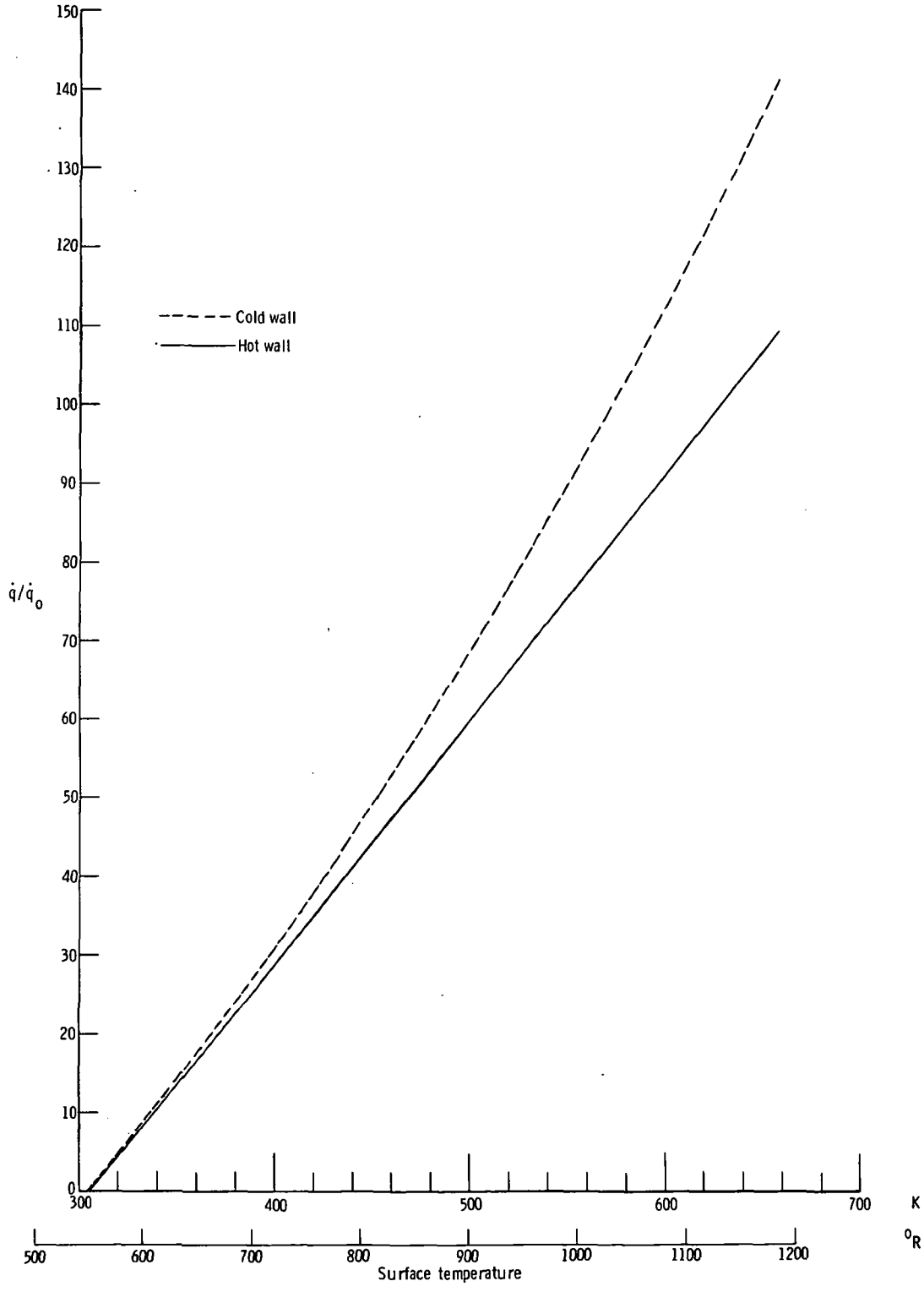

Figure 14.- Surface heating rate as a function of surface temperature calculated using code of reference 9. $\dot{q}_o$ = 11.35 kW/m^2 (1.0 Btu/ft^2-sec); 1.27-cm (0.5-in.) thick stainless steel plate; initial temperature, 305.6 K (550° R).

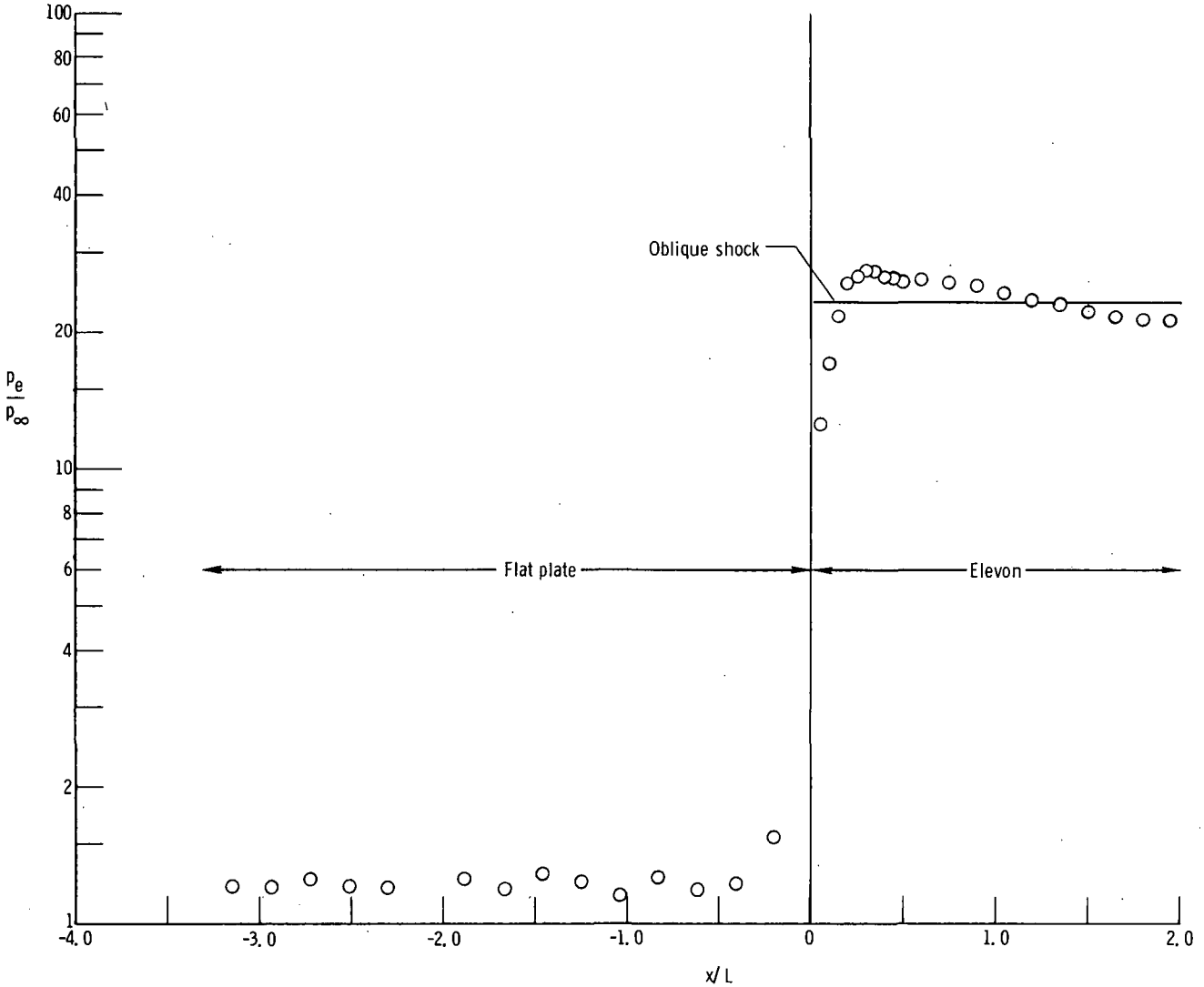

Figure 15.- Pressure distribution for test run 1 on flat plate and elevon. M_∞ = 7.0; q_∞ = 49.7 kPa (1037 psf); ε = 30°; α = 0°.

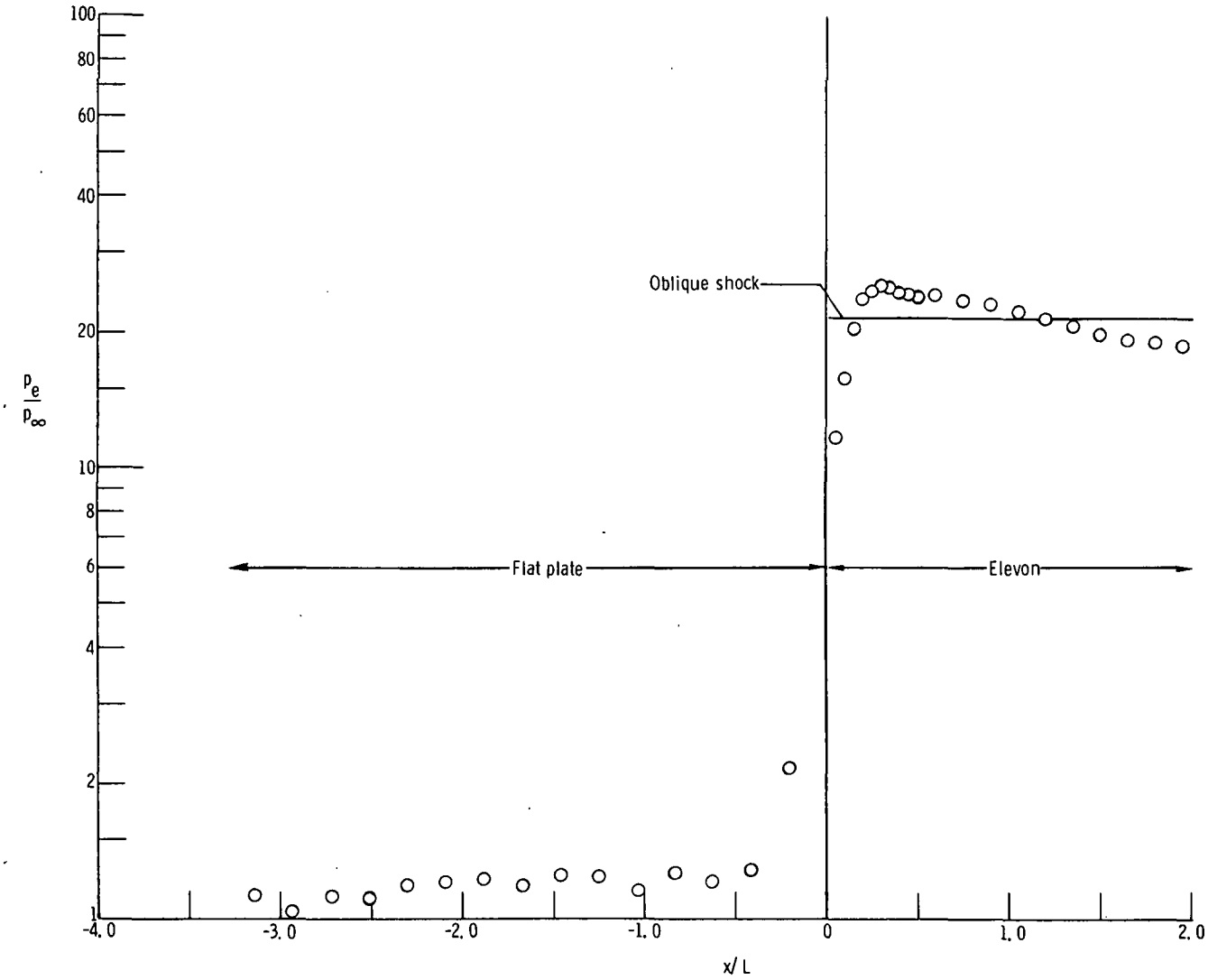

Figure 16.- Pressure distribution for test run 2 on flat plate and elevon. $M_\infty = 6.7$; $q_\infty = 61.1$ kPa (1275 psf); $\epsilon = 30^\circ$; $\alpha = 0^\circ$.

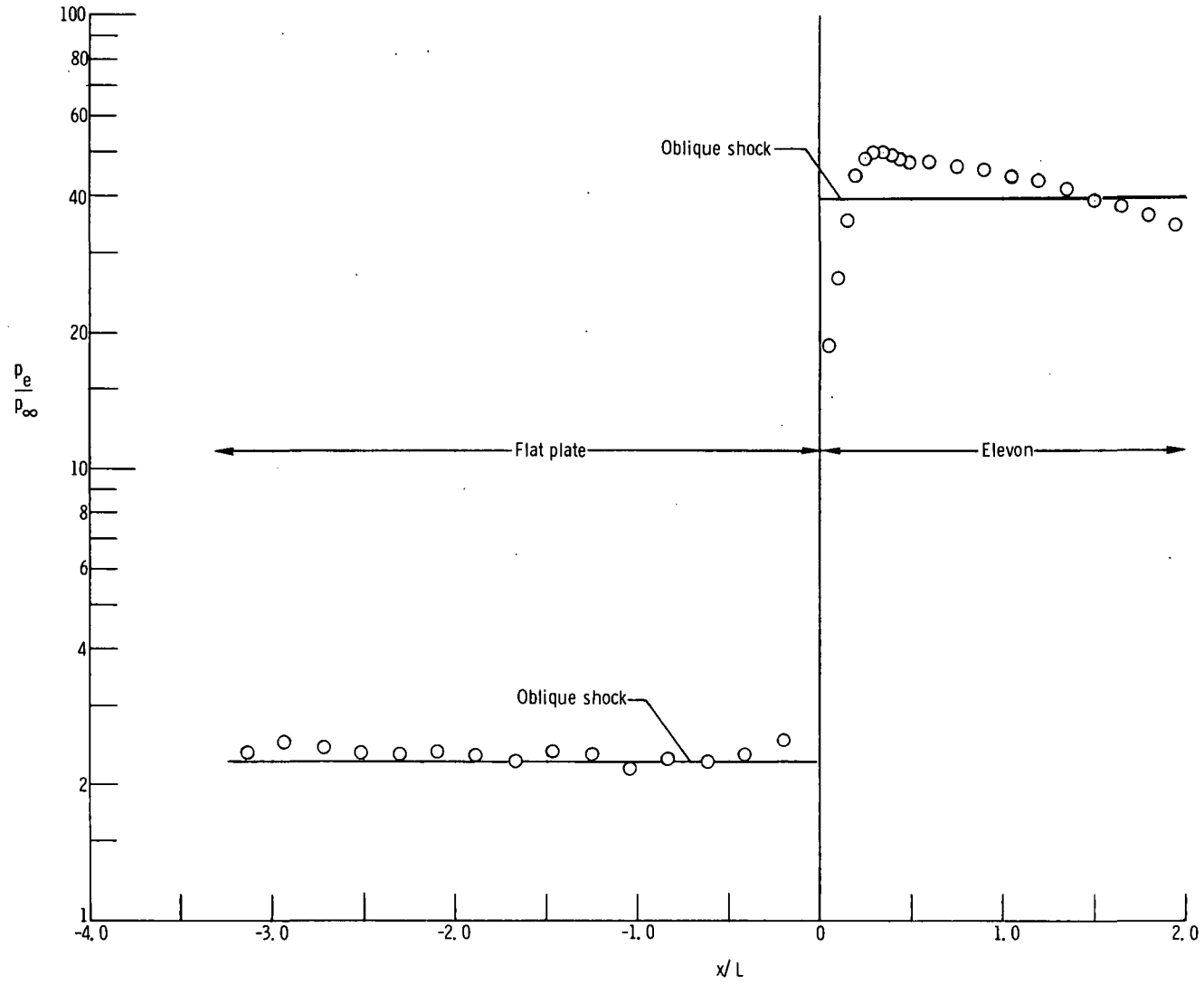

Figure 17.- Pressure distribution for test run 3 on flat plate and elevon. $M_\infty = 6.9$; $q_\infty = 48.5$ kPa (1013 psf); $\varepsilon = 30^\circ$; $\alpha = -5^\circ$.

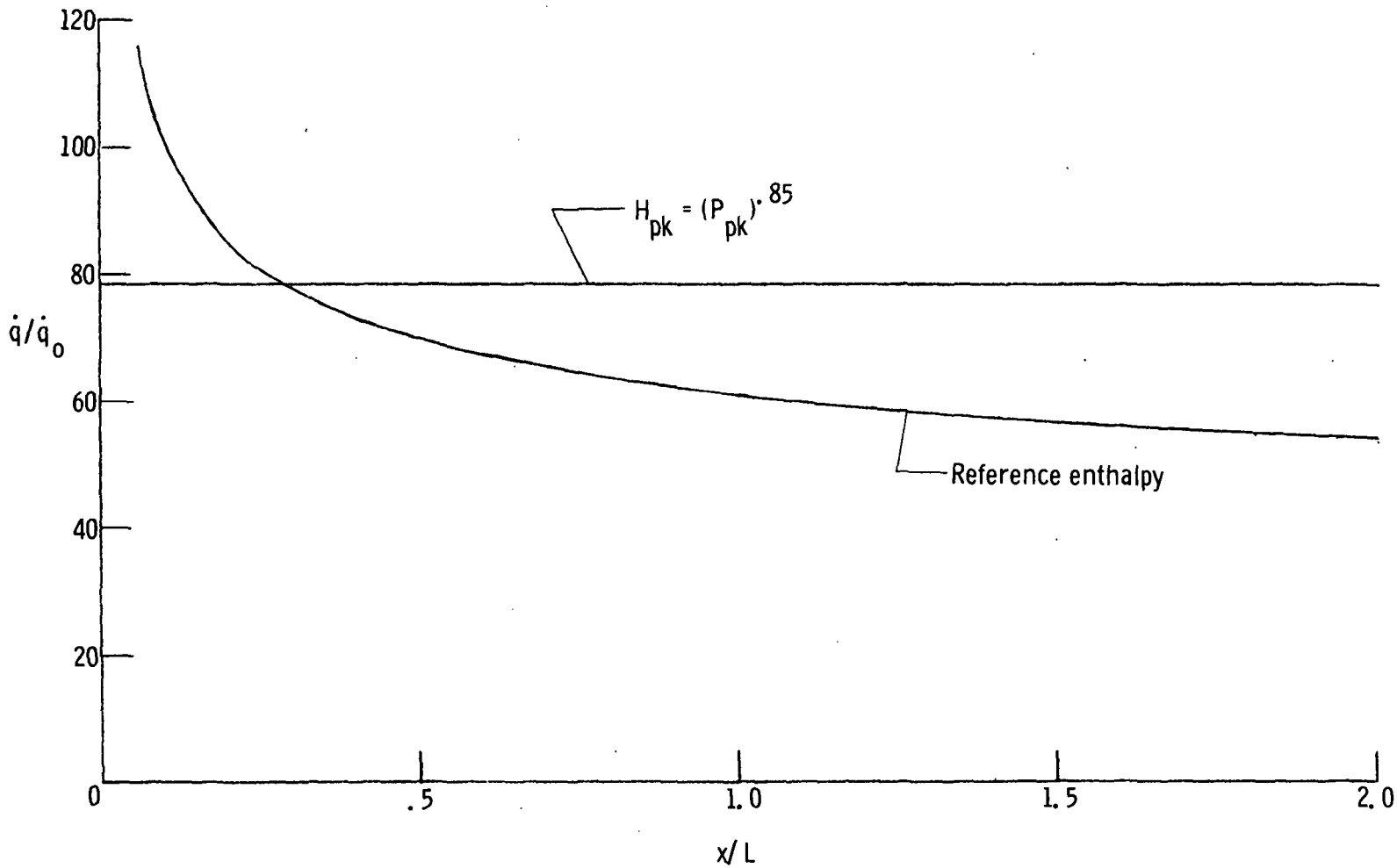

Figure 18.- Calculation of heating to elevon deflected 30° at flight conditions of $M_\infty = 6.9$ and $q_\infty = 47.9$ kPa (1000 psf). $\dot{q}_o = 11.35$ kW/m^2 (1.0 Btu/ft^2-sec).

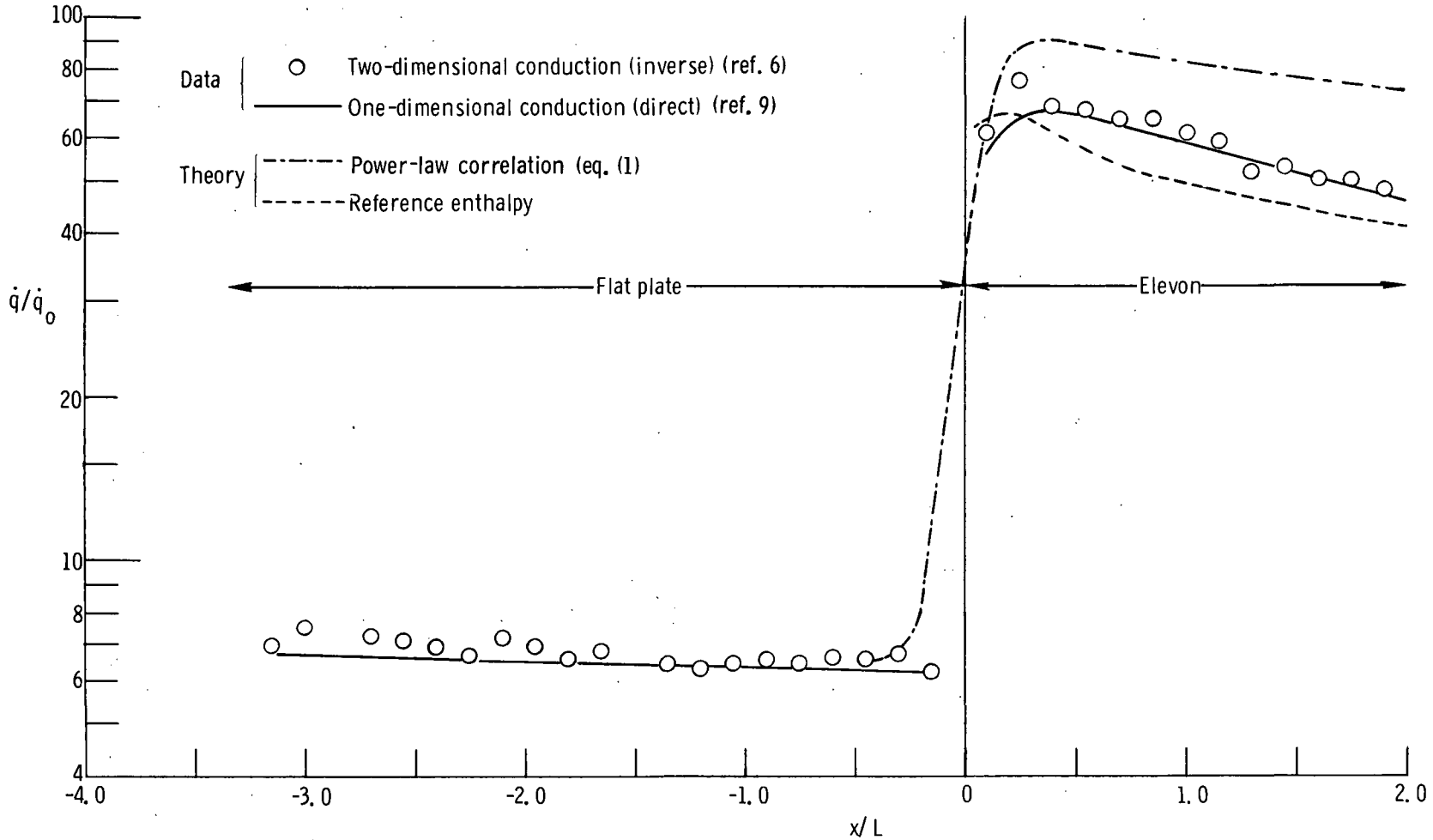

Figure 19.- Heat-transfer distribution for test run 1 on flat plate and elevon.
M_∞ = 7.0; q_∞ = 49.7 kPa (1037 psf); ε = 30°; α = 0°; t = 4.0 sec;
$\dot{q}_o$ = 11.35 kW/m^2 (1.0 Btu/ft^2-sec).

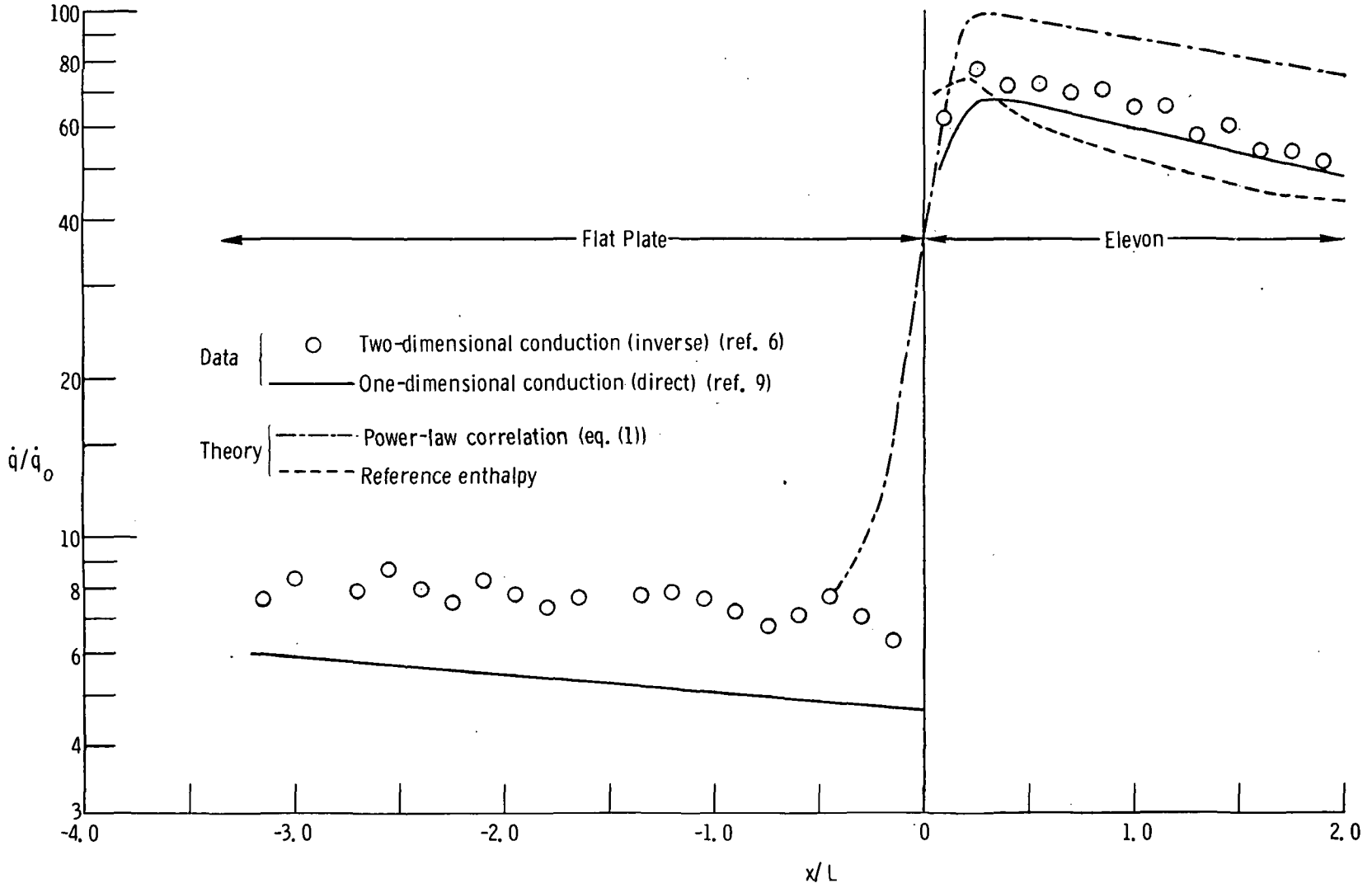

Figure 20.- Heat-transfer distribution for test run 2 on flat plate and elevon.
M_∞ = 6.7; q_∞ = 61.1 kPa (1275 psf); ε = 30°; α = 0°; t = 4.0 sec;
$\dot{q}_o$ = 11.35 kW/m^2 (1.0 Btu/ft^2-sec).

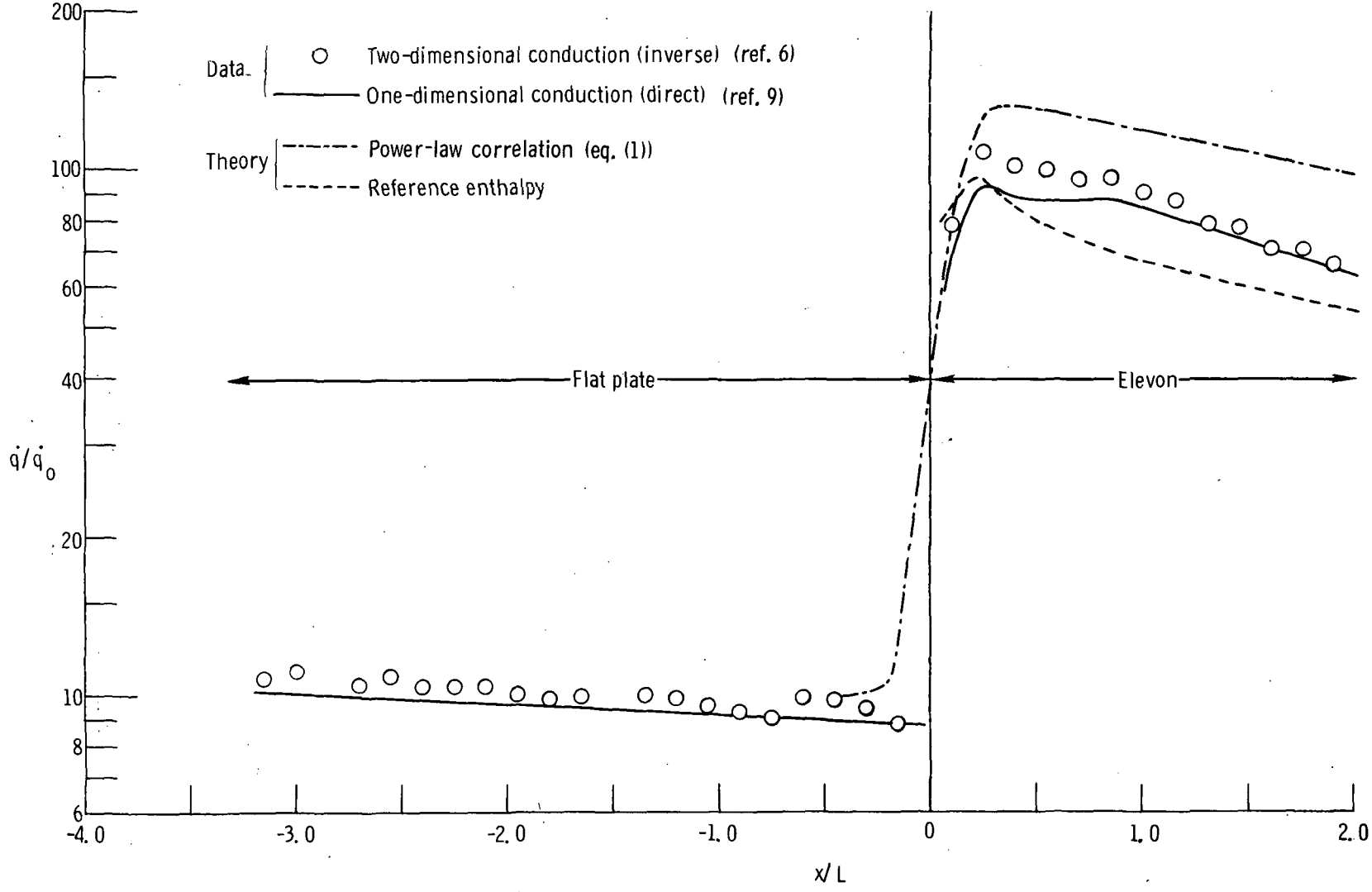

Figure 21.- Heat-transfer distribution for test run 3 on flat plate and elevon. $M_\infty = 6.9$; $q_\infty = 48.5$ kPa (1013 psf); $\varepsilon = 30^\circ$; $\alpha = -5^\circ$; $t = 4.0$ sec; $\dot{q}_o = 11.35$ kW/m^2 (1.0 Btu/ft^2-sec).

"The aeronautical and space activities of the United States shall be conducted so as to contribute . . . to the expansion of human knowledge of phenomena in the atmosphere and space. The Administration shall provide for the widest practicable and appropriate dissemination of information concerning its activities and the results thereof."

—NATIONAL AERONAUTICS AND SPACE ACT OF 1958

NASA SCIENTIFIC AND TECHNICAL PUBLICATIONS

TECHNICAL REPORTS: Scientific and technical information considered important, complete, and a lasting contribution to existing knowledge.

TECHNICAL NOTES: Information less broad in scope but nevertheless of importance as a contribution to existing knowledge.

TECHNICAL MEMORANDUMS: Information receiving limited distribution because of preliminary data, security classification, or other reasons. Also includes conference proceedings with either limited or unlimited distribution.

CONTRACTOR REPORTS: Scientific and technical information generated under a NASA contract or grant and considered an important contribution to existing knowledge.

TECHNICAL TRANSLATIONS: Information published in a foreign language considered to merit NASA distribution in English.

SPECIAL PUBLICATIONS: Information derived from or of value to NASA activities. Publications include final reports of major projects, monographs, data compilations, handbooks, sourcebooks, and special bibliographies.

TECHNOLOGY UTILIZATION PUBLICATIONS: Information on technology used by NASA that may be of particular interest in commercial and other non-aerospace applications. Publications include Tech Briefs, Technology Utilization Reports and Technology Surveys.

Details on the availability of these publications may be obtained from:

SCIENTIFIC AND TECHNICAL INFORMATION OFFICE

NATIONAL AERONAUTICS AND SPACE ADMINISTRATION

Washington, D.C. 20546